5-1-2012

Hydro/Solvothermal Synthesis, Structures and Properties of Metal-Organic Frameworks Based on S-Block Metals

Raj Kishore Vakiti
Western Kentucky University, raj.vakiti254@topper.wku.edu

HYDRO/SOLVOTHERMAL SYNTHESIS, STRUCTURES AND PROPERTIES OF METAL-ORGANIC FRAMEWORKS BASED ON S-BLOCK METALS

A Thesis
Presented to
The Faculty of the Department of Chemistry
Western Kentucky University
Bowling Green, Kentucky

In Partial Fulfillment
Of the Requirements for the Degree
Master of Science

By
Raj Kishore Vakiti

May 2012

HYDRO/SOLVOTHERMAL SYNTHESIS, STRUCTURES AND PROPERTIES OF METAL-ORGANIC FRAMEWORKS BASED ON S-BLOCK METALS

Date Recommended 4-17-2012

Dr. Bangbo Yan, Director of Thesis

Dr. Cathleen Webb

Dr. Yan Cao

Dr. Wei-Ping Pan

Dean, Graduate studies and Research Date 4-June-2012

I dedicate the thesis to my family, friends and to Dr. Bangbo Yan who supported and encouraged me the most during my challenging times here at Western Kentucky University.

ACKNOWLEDGMENTS

I wish to express my hearty thanks and appreciation for the contribution and help of the many people who made this work possible: I would like thank my parents Raja Reddy Vakiti and Jaya Reddy Vakiti for their support and guidance; Dr. Bangbo Yan, for his everlasting support and patience; Dr. Wei-Ping Pan and Dr. Yan Cao, for their timely guidance and also for helping me for the analysis of materials for my research; Dr. Cathleen Webb, for giving me the right advice in order to accomplish my goals; Dr. Rajalingam Dakshinamurthy, for giving suggestions; Ms. Alicia McDaniel, for her support and help; Ms. Shannon Marble and Ms. Aly Anderson for always helping me and making things easier and enjoyable; I wish to thank Dr. Houyin Zhao for her help in analysis. I would like to thank my research group members Yanfen Li and Nithin Pally for their support and suggestions.

I would like to especially thank Dr. Bangbo Yan, for giving me an opportunity to work in his research group and for providing such a good research project. He supported me until the completion of my research.

TABLE OF CONTENTS

List of Figures VI

List of Tables IX

Abstract X

Chapter One: Introduction 1

Chapter Two: Literature Review 4

Chapter Three: Methods and Instruments 21

Chapter Four: Synthesis and characterization of two- and three-dimensional calcium coordination polymers built with benzene-1, 3, 5-tricarboxylate and/or pyrazine-2-carboxylate …..... 32

Chapter Five: Two Novel Three-Dimensional Metal-Organic Frameworks Using s-Block Metal Ions as Nodes 59

Chapter Six: Conclusion 77

LIST OF FIGURES

Figure 3.1(a) The parts of the autoclaves (b) the entire setup the autoclave 21

Figure 3.2 ARL Thermo X-ray Diffractometer 23

Figure 3.3 Bruker Quazar diffractometer.....25

Figure 3.4 TA Q5000 Thermogravimetric Analyzer 26

Figure 3.5 PerkinElmer LS55 fluorescence spectrophotometer 27

Figure 3.6 Cary 100 UV-vis spectrophotometer.....28

Figure 3.7 Perkin Elmer Spectrum One FTIR spectrometer.....29

Figure 4.1 (a) The asymmetric unit; (b) the coordination environment of Ca (1); (c) the coordination environment of Ca(2); and (d) the coordination environment of btc in compound **1**.....39

Figure 4.2 (a) The helical chain in compound 1; (b) the layer in **1** formed by helical c hains linked through Ca(2); (c) the 3D structure of **1** formed by bridging water molecules between neighboring layers 40

Figure 4.3 (a) The asymmetric unit; (b) the coordination environment of Ca(1); (c) the coordination environment of Ca(2); and (d) the coordination environment of btc and pzc in compound **2** 42

Figure 4.4 (a) The zigzag chain in compound **2**; (b) The zigzag chain with ligands in compound **2**; (c) the 2D structure of **2** formed by bridging btc ligands between neighboring layers (hydrogen bonds are shown in dash lines 43

Figure 4.5 Experimental (b) and simulated (a) powder X-Ray patterns of compound **1**...44

Figure 4.6 Experimental (b) and simulated (a) powder X-Ray patterns of compound **2**...45

Figure 4.7 Thermogravimetric analyses of compounds **1** and **2**.....46

Figure 4.8 UV-vis spectra of free Hpzc ligand in aqueous solution.....48

Figure 4.9 UV-vis Diffuse reflectance spectra of Hpzc.....48

Figure 4.10 UV-vis spectra of H_3btc in aqueous solution 49

Figure 4.11 UV-vis Diffuse reflectance spectra of H_3btc 49

Figure 4.12 UV Diffuse reflectance spectra of compounds **1** and **2**.....50

Figure 4.13 The excitation-emission spectra of (a) compound **1** and (b) compound **2** at room temperature 51

Figure 4.13.1 The emission and excitation spectra of free ligand H_3btc 53

Figure 4.13.2 The emission and excitation spectra of free ligand Hpz.....53

Figure 4.14 IR spectra of compound **1** (KBr).....54

Figure 4.15 IR spectra of compound **2** (KBr).....55

Figure 5.1 a) Asymmetric unit; b) the coordination Ca; c) coordination of btc environment; d) 1D inorganic chain of {CaO_8} 64

Figure 5.2 3D crystal structure of compound 6 67

Figure 5.3 (a) Asymmetric unit; (b) bdc coordination environment; (c) rubidium coordination environment 68

Figure 5.4 The 3D crystal structure of the compound **7** 68

Figure 5.5 The Thermogravimetric analyses of compounds **6** and **7** 70

Figure 5.6 The excitation-emission spectra of compound **6** and compound **7** at room temperature 71

Figure 5.7 IR spectra of compound **6** 73

Figure 5.8 IR spectra of compound **7** 74

LIST OF TABLES

Table 3.1 Different chemical materials.....30

Table 4.1 Crystal data and structure refinements for compounds **1** and **2**.....37

Table 4.2 Selected Bond Lengths [Å] for compounds **1** and **2**.....38

Table 5.1 Crystal data and structure refinements for compounds **1** and **2**.....66

HYDRO/SOLVOTHERMAL SYNTHESIS, STRUCTURES AND PROPERTIES OF METAL-ORGANIC FRAMEWORKS BASED ON S-BLOCK METALS

Raj Kishore Vakiti May 2012 77 Pages

Directed by: Dr. Bangbo Yan, Dr.Yan Cao, Dr.Cathleen Webb and Dr.Wei-Ping Pan

Department of Chemistry Western Kentucky University

Carbon dioxide removal from flue gases of power plants is critical for reduction of greenhouse gas emissions implicated in global warming. Metal Organic Frameworks (MOFs) promising potential applications in carbon dioxide capture due to their unique structural properties such as high porosity and high thermal stability. These MOFs have application in separation processes and gas storage. By the assembly of the organic ligands and metal oxide clusters, porous MOFs can be synthesized. The use of s-block metals such as calcium, magnesium and rubidium in porous materials is appealing because their ionic binding characters with organic ligands will general flexible MOFs. The bonding interaction of s-block metal centers with carboxylate oxygen atoms is mainly ionic in nature due to large differences in electronegativity. The s-block elements can form low density frameworks which could increase the gas uptake capacity of small molecules.

This work focuses on synthesis of new metal organic frameworks (MOFs) using s-block metals. Different types of the carboxylic ligands were utilized for synthesis of MOFs. Four new calcium or rubdium metal organic frameworks, $[Ca_3(btc)_2(H_2O)_{12}]$ (**1**) and $[Ca_2(btc)(pzc)(H_2O)_3]$ (**2**) (btc=benzene-1,3,5-tricarboxylate, pzc = pyrazine-2-carboxylate), $[Ca(Hbtc)(H_2O)]\bullet H_2O$ (**6**), and [Rb(Hbdc)] (**7**) have been synthesized using the hydro/solvothermal method and have been characterized using X-ray diffraction, IR, UV-vis, TGA and fluorescence analysis. The structures of compounds **1**,

6 and **7** are three-dimensional frameworks while that of compound **2** is a double layered network.

Chapter 1

Introduction

Carbon dioxide (CO_2) emissions from industrial processes contribute to global warming, sea level rise, and an irreversible increase in the acidity levels of the oceans with undesirable impact on the environment.[1] These potential threats have led many scientists and others to conclude that action is necessary to reduce greenhouse gas levels, in particular levels of carbon dioxide in the atmosphere.

In this regard, porous solids have recently received particular attention for their potential applications as sorbents in CO_2 separations.[2] Conventional porous materials such as zeolites and carbon nanotube materials for separation of CO_2 have disadvantages such as high cost and difficulty in recycling.[3-6] Recently metal-organic frameworks (MOFs) have attracted attention as adsorbents owing to their high surface area, low densities, and high porosity, thermal stability and adjustable chemical functionalities.[7]

MOFs are crystalline solids composed of metal ions (normally called nodes) linked by organic ligands (as linkers). These materials often form three-dimensional extended frameworks with porous structures. The linkers are often organic molecules with specific functional groups such as carboxylate, pyridyl that can coordinate to metal nodes such as Zn, Cu, Fe. Porous MOFs are promising materials for CO_2 capture because of their unique properties such as robustness, high thermal and chemical stabilities, exceptional internal surface areas, high pore volumes, and low densities in comparison with traditional porous materials. For example, MOFs may possess active surface area of

up to 1500–4500 m^2g^{-1}, while activated carbon 400-1000 m^2g^{-1} and zeolites up to 1500 m^2g^{-1}. [8] Moreover, the pore dimensions and surface chemistry of MOFs can be systematically modulated by modifying the organic ligands or changing metal ions used in the synthesis of these materials.

The challenge in design and development of MOFs for CO_2 capture, as pointed out by Long et al, is the selectivity of MOFs on CO_2 over other gas molecules, inverse relationship between the adsorption and diffusion selectivity, and the adsorption capacity. Moreover, the costs of using MOFs as sorbents are considered as a major issue to address.[9]

In contrast to the large amount of MOFs built from transition metal ions reported in the literature, there are a relatively limited number of examples based on s-block metals.[10]The use of s-block metals such as calcium and magnesium in porous materials is appealing because their ionic binding characters with organic ligands will generate flexible MOFs. It is also been shown that doping alkaline earth metals or alkaline metals in MOFs may enhance their ability for gas storage due to the stronger binding capability of these metals to certain gases such as CO_2 or H_2. The aim of this research is to synthesize new metal-organic frameworks using s-block metals and carboxylate ligands, with potential applications in CO_2 capture.

REFERENCES

1) Pachauri, R. K.; Reisinger, A. Climate Change 2007, *IPCC*, Geneva, Switzerland, **2008**.

2) Jagadeswara, R. K.; Krista, S. W. *Langmuir*, **2008**, 24, 16.

3) Goj, A.; Sholl, D. S.; Akten, E. D.; Kohen, D. *J. Phys Chem B*, **2002**, 106, 8367.

4) Bernal, M. P.; Coronas, J.; Menendez, M.; Santamaria, J. *AICHE J*, **2004**, 50, 127.

5) Akten, E. D.; Siriwardane, R. V.; Sholl, D. S. *Energy Fuels*, **2003**, 17, 977.

6) Yang, R. T.; Adsorbents: Fundamentals and Applications, *John Wiley& Sons*, Inc. Hoboken, **2003**.

7) Snurr, R. Q.; Hupp, J. T.; Nguyen, S. T. *AICHE J*, **2004**, 50, 1090.

8) Rowsell, J. L. C.; Yaghi, O. M. *Microporous Mesoporous* Mater, **2004**, 73, 3.

9) Kitagawa, S.; Kitaura, R.; Noro, S. *Angew Chem, Int.Ed*, **2004**, 43, 2334.

10) Electric Power Research Institute, Program on Technology Innovation: Post combustion CO2 Capture Technology Development, Palo Alto, **2008**.

Chapter 2

Literature Review

1. Introduction

Metal-organic Frameworks (MOFs) are crystalline solids with infinite network structures that are built from metal ions and organic bridging ligands. Over the past decade, porous MOF materials have captured the attention of many research groups all over the world because of their exceptional properties such as high surface area, low densities, high porosity, thermal stability and adjustable chemical functionalities.[1] This chapter will give a brief review of porous materials including MOFs and Zeolites.

2. Zeolites

Porous solids can be classified into three categories based on sizes of their pores: microporous, mesoporous and macroporous materials. Solids which have a pore size of 2 nm or below are known as microporous.[3] The mesoporous solids are in the range of 2 nm–50 nm and above 50 nm are known as macroporous.[4,5]

Zeolites are traditional inorganic microporous crystalline materials.[6,7] Zeolites were discovered in 1756 in Sweden and they are oldest known porous materials.[14] Zeolite structures are composed of tetrahedral $Si(Al)O_4$ units covalently joined by bridging O atoms to produce different types of frameworks.[15] Zeolites have been used as host materials that have been developed into new nanocomposites with optical[8-11] , magnetic,[12] or electrical[13] properties.

Zeolite materials have applications such as ion exchanges in laundry detergents and water softeners removing unwanted ions in the water.[16] Zeolites are typically used in molecular separations of small molecules by selecting an appropriate sieve with an adequate pore size to bind a particular molecule such as water. These zeolite adsorbents with particular pore size, pore shape, and chemical functionality provide significant advance in areas such as adsorption separations and catalysis.[17]

3. AlPOs and Mesoporous Materials

Microporous aluminophosphate materials (AlPO-n) were reported as the first example of inorganic molecular sieves and composed of material other than aluminosilicates. Their frameworks are composed of both tetrahedral AlO_4 and PO_4 units and some materials have novel structures. The physicochemical properties of these materials are attractive and interesting.[3] After the first preparation of AlPOs, interest in these materials as adsorbent, catalysts or catalyst are increasing.[2] High thermal stability and easy incorporation of hetero elements are the attractive properties of these materials. Incorporation of divalent metals in the aluminophosphate molecular sieves imparts the acidity, ion exchange capacity and enhanced hydrophilicity. [18]

The mesoporous silicates or aluminoslicates with pore size ranging from 2 nm-10 nm are prepared using surfactants as surface directing agents under hydrothermal conditions. Using cationic surfactants, mesostructured aluminophosphates were also synthesized and hexagonal phases were also reported as silico aluminophophates.[19-25] These mesostructures have problems of low thermal stability. Because of this, other frameworks with high thermal stability and high pore size should be developed. In recent

years the interest on metal-organic frameworks has been increasing because of their attractive properties.

4. Porous Metal Organic Frameworks

MOFs are a recent addition to the porous material family and they provide a new platform for developing novel functionalized materials. MOFs with exceptional properties make them the promising materials for adsorption separations, gas storage, catalysis and sensing.[26]

Design and Synthesis of MOFs

MOFs can be synthesized by self-assembly of organic ligands and metal ions.[19] There are two ways to tune the pore size and provide desired surface chemistries: 1) direct assembly of new MOFs from particular metal nodes and organic linkers and 2) the pre-constructed robust precursor MOFs are modified by the post-synthesis.[27] The flexible ways of making MOFs have led to synthesis of thousands of MOFs during recent years.

MOFs can be built from two types of building units: metal ions and organic ligands. The pore volume and surface area of MOFs can be controlled by modifying organic ligands which act as spacers and create an open porous structure.[28]

Metal Ions as Building Units of MOFs

Metal ions, with a preferred coordination number and geometry, in combination with divergent linker molecules can create extended networks in one, two, or three dimensions. First row transition metals are well known to be able to coordinate with carboxylate groups under hydro and solvothermal conditions and these metal centers are

often chosen because of the coordination properties of these transition metals. MOFs based on s-block metal centers are relatively less known and study on these metal centers is increasing because these metals have lower density compared to transition metal centers and the other group metals. The bonding interaction of s-block metal centers with carboxylate oxygen atoms is mainly ionic in nature due to large differences in electronegativity, which makes it hard to predict and control over coordination geometry.[29]The s-block metal ions have disadvantages such as lack of predictive coordination behavior and the dominance of steric considerations. Apart from that, incorporation of s-block metal ions into frameworks offers several advantages like the strong bonding interaction with carboxylate oxygen atoms because of high charge density and ionic nature of these metal ions. The porous frameworks prepared from early members of the metal ions of s-block provide gravimetric advantages for gas-storage applications due to their low-atomic weight. Frameworks constructed from s-block metals like Na, Ca, Mg, K are cheap, non-toxic and useful in biological processes.[30]

The different types of the s-block metals have been used in synthesis of low density networks. The metal coordination and linker geometry is discussed in forming different types of MOFs of some s-block metals.

Calcium

The larger size of Ca^{2+} compared with Mg^{2+} leads to higher coordination numbers, while the structural topologies of the networks formed are equally dependent on the chemical nature and geometry of the ligands. The variation in coordination numbers is due to the presence of different numbers of water molecules in the coordination sphere.

The use of larger polycarboxylate aromatic linkers, [32-34] including naphthalene or biphenyl based polycarboxylates, results in 3-D dense networks with Ca-carboxylate oxygen based chains or layered motifs. Solvent molecules (water, Dimethyl formide (DMF), Diethyl formide (DEF)) are often involved in the metal coordination sphere.

Rubidium

The large electronegativity difference between the Rb metal center and carboxylate oxygen atoms impose strong ionic character on the M-O bonds of the MOFs. The coordination of rubidium is that it binds to two or more functional groups of organic linkers. Ferey and co-workers[35] recently reported 3D Rb/Cs CNs with redox-active tetrathianfulvalene tetracarboxylate (TTF-TC)as the organic linkers, forming networks of general formula M_2(TTF-TC)H_2 (M = Rb, Cs). Each tetrahedrally coordinated ^{IV}Rb is interconnected through the linkers to form the overall 3-D network. Under solvothermal conditions a dense 3-D ^{VI}Rb/^{VII}Rb coordination network using BTC linkers have been reported by Kim and co-workers[31].The network contains channels with edge sharing RbO_6 and RbO_8 polyhedral chains surrounding it, connected by the organic linkers.

Magnesium

Magnesium is the s-block metal used to build metal organic frameworks. Like Zn^{2+}, Mg^{2+} is commonly observed to adopt octahedral coordination, has a comparable ionic size (0.72 Å for Mg^{2+} 0.74 Å for Zn^{2+}), and has a similar affinity for rigid aromatic carboxylate linkers. Assembling networks based on a lightweight metal center Mg^{2+}, rather than Zn^{2+}, offers gravimetric advantages for gas storage applications.[35]

Organic Ligands as Building of MOFs

The MOFs are prepared by secondary binding units (SBUs) such as 1,4 benzenedicarboxylate (BDC) and 1,3,5-benzenetricarboxylate (BTC) which offers advantages due to their rigidity and consequent tendency to form rigid metal carboxylate clusters. The choice of ligand is particularly important because the structure and length of the ligand will directly affect the size and architecture of the framework.

Ligands with this linear orientation are known to generate square planar or cubic MOFs in the presence of transition metal ions. Many MOFs reported in the literature have a cubic architecture composed of orthogonal intersecting channels exposed at the

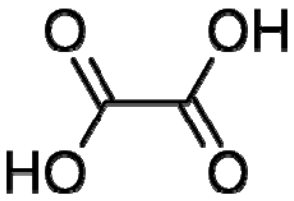

Pyrazine-2-carboxylic

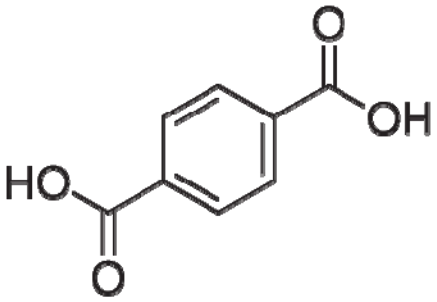

Benzene-1, 4 -dicarboxylic acid

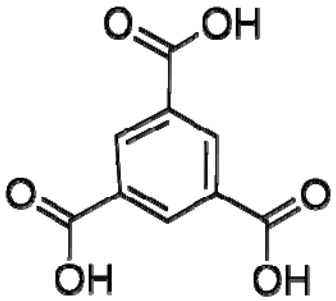

Benzene-1, 3, 5-tricarboxylic acid

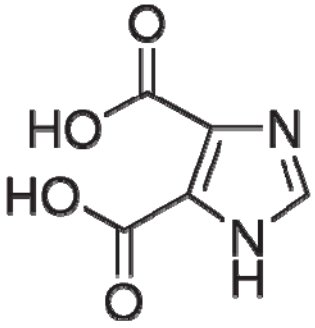

4, 5-Imidazole dicarboxylic acid

faces of the cube through which guest solvents can pass.

Open Metal Sites in MOFs

In some MOFs, metal atoms are partially coordinated by solvent molecules from the synthesis. It is important to activate MOFs at elevated temperature to remove the solvent and open the void space for desired guest molecules. Removing these coordinated solvent molecules leaves coordinatively unsaturated open-metal sites that have been shown to promote high gas uptake, especially for H_2 adsorption.[36-45] The open space created after removal of coordinated solvent molecules is called open metal site. Bae et al [48] showed that in a carborane-based MOF, removal of coordinated dimethylformamide (DMF) increased CO_2 and CH_4 adsorption and led to high selectivity for CO_2 over CH_4. [46]

Open metal sites found in Cu-BTC[46] and MIL-100, [47] have been shown to impart the catalytic activity to the materials. From this concept it can be expected that adsorption selectivity can be enhanced. [19]

Thermal Stability of MOFs

The adsorption of gases depends on the stability of MOFs and the different types of stabilities of these materials are thermal and structural stability. The materials with high thermal stability can be used for adsorption of gases at high temperatures. The structural stability of MOFs is a very important factor. The structure of the materials should be stable upon exposure to high temperatures. If the structure of the material is affected, it leads to changes in the surface area, pore size and pore volume. The

adsorption of the gases decreases depending on the pore size. The different methods used to determine the stabilities are thermo gravimetric analysis to determine the thermal stability of the material and Powder X-ray Diffraction for the purity and structure. Zeolites have high thermal stability compared to MOFs but these materials require high temperatures for regeneration of adsorbents and they can be used only in shape selective separation of gases. Because their pores are like molecular sieves which can absorb only certain specific gases, understanding the multicomponent adsorption equilibrium is essential for designing adsorption-based separation processes. The MOFs have an additional advantage as they can be regenerated under milder conditions than most zeolites which require considerable heating and high costs.[48] Many of the publications focused on single component gases, so further studies should focus on the mixture behavior of gases. The disadvantages of MOFs are they are not stable when heated at very high temperatures and decomposition on exposure to more than 4% wt water. MOFs with stable structure upon exposure to moisture should be developed.

5. Applications of MOFs

In the recent years, many research groups are interested in MOFs because of their high adsorption capacity, pore size, surface area and high volume. MOFs are nano porous materials that have potential applications in gas purification, gas separation, gas storage, catalysis and biomedical applications.

The use of metal-organic frameworks for separation or storage of carbon dioxide has many advantages over the other commonly used techniques like carbon capture and separation (CCS), chemical adsorption by amine solutions and pressure-swing adsorption

(PSA). The CCS technologies are high cost processes and require more energy. Adsorption-based separations such as pressure-swing adsorption are interesting due their low energy requirements but an adsorbent with high CO_2 selectivity is essentials for PSA processes.[62] Chemical adsorption processes posses disadvantages like high energy requirements for regeneration of adsorbents, loss of effectiveness over time due to low thermal stability, loss due to evaporation, and a tendency to induce corrosion. The MOFs posses extremely high surface area and high pore volume. These materials can be synthesized inexpensively, relatively easily, in high purity and in a highly crystalline form.[63]

5.1 Gas purification

MOFs are useful materials for the purification of the traces of chemical components from various gases. MOFs can be used in removal of ppm level sulfur components from various gases. MOF structures with accessible open metal sites are well suited to strongly (430 kJ mol^{-1}) chemisorb electron-rich, odour-generating molecules, like amines, phosphines, oxygenate, alcohols, water, or sulfur containing molecules.[49]

The removal of tetrahydrothiophene (THT, odorant) from natural gas at room temperature, 10–15 ppm sulfur were fully down to less than 1 ppm using an electrochemically prepared shaped Cu-EMOF in a fixed bed reactor.[50]

5.2 Gas storage

The MOFs are unique structures and have high capacity to store various gases. The increase in the volume of specific storage depends on the type, temperature and pressure of the gas, as well as on the specific MOF material being used.

Hydrogen is one of the important gases of the future as an energy carrier because of its clean burning and high energy content. Many reports have dealt with the use of hydrogen as a fuel instead of gasoline fuels and it's storage in different solid-state media and in high-pressure or cryogenic tanks.[51] There are two problems for the storage of hydrogen and transportation of the gas. First, the transportation of hydrogen through vehicles is one of the problems because the transportation sector requires fuel oil and thus it is the largest sources of air pollutants. Secondly, to make the hydrogen competitive with fossil fuel is more challenging than for stationary storage. The current target of theU.S. Department of Energy (DOE) has been made with the concept of using the hydrogen as the gasoline fuel. The vehicles should have the similar range (480 km or 300 miles), operate close to ambient conditions , and be quickly and safely refueled.[52] As the hydrogen contains three times the energy of the gasoline per unit mass, it was estimated that the hydrogen storage tank can carry 5 kg of H_2. The goals for 2015 are 9 wt% and 81kg H_2 per m^3, which approach the expectations of the automotive industry.[53] MOFs with large pores may not be good for H_2 storage due to poor attraction from the surface of pore walls where the H_2 molecule located in the center of the pore. Therefore, MOFs with pores just bigger than the kinetic diameter of the H_2 would be an ideal storage material.[54]

The best example for H_2 storage is MOF-5, which is a cubic Zn-terephthalate based network. It shows a gravimetric uptake of about 1.3 wt% at 1 bar and 5.1 wt% at 5 bar at 77K.[55] This may be due to incomplete removal of guest molecules. Upon complete activation the H_2 uptake observed was 7.1 wt% at 77 K and 40 bar. This amount increased to 10 wt% at 100 bar which corresponds to the volumetric storage density of 66 g L^{-1}.

Although MOF-5 shows high storage capacity at 77 K, it does not show a good uptake at 298 K due to weak interactions between H_2 and the framework. This shows that MOF-5 is not a good material for H_2 storage. Apart from hydrogen gas, the adsorption of small molecules like N_2, CO, CO_2 and Ar are successful. The goals set by U.S.Department of Energy were not met by any of them and the hydrogen economy is yet to flourish.

5.3 Gas separation

Gas separation is a process which separates the mixtures of gases into single components. MOFs are potential materials for gas separation because they have high surface area, adjustable pore sizes and controllable surface properties. MOFs pores can be altered by design but in zeolites pores are difficult to alter due to its rigid tetrahedral oxide skeletons. The separation of gas from mixture of gases is important because if one gas is harmful for atmosphere, it is important to remove that gas instead of removing all the gases. For example, the removal of carbon dioxide (CO_2) and methane (CH_4) from natural gas is important because these two are harmful gases to the atmosphere which leads to global harming.

Gas adsorptive separation of porous materials can be achieved because of:

(1) size and/or shape exclusion which means certain components of a gas mixture are prevented from entering the pores of an adsorbent while other components are allowed to enter the pores where they are subsequently adsorbed, known as the molecular sieving effect.

(2) different adsorbate-surface and/or adsorbate packing interactions which means preferential adsorption of certain components over others occurs on the surface of an adsorbent, known as the thermodynamic equilibrium effect.

(3) different diffusing rates which means certain components enter the pores and become adsorbed faster than other components, known as the kinetic effect.

(4) the quantum effect which means some light molecules have different diffusing rates in narrow micropores, which allows such molecules to be separated, known as the quantum sieving effect.

The different techniques used for the separation are distillation, pressure or thermal swing adsorption-desorption and membrane based separation.[56] Nitrogen–oxygen (air), nitrogen–methane, and noble gas (e.g. Kr–Xe) separations are examples of separation technologies in which zeolitic adsorbents are used. Recently, the separation of Kr–Xe by pressure swing adsorption as well as the purification of methane in natural gas, was piloted on MOF-adsorbents.[57, 58]

For example, removal of tetrahydrothiophene (THT) from natural gas has been studied at room temperature.[60] An electrochemically prepared fixed bed reactor has been used for this purpose and is filled with Cu-EMOF. About 10-15 ppm traces of sulfur was

able to to be decreased to less than1 ppm from this process. MOFs with accessible open metal sites are well suited for the separation process.[59]

5.4 Biomedical Applications

The biomedical applications of MOFs have also been investigated. Stability and toxicology of the materials are the main issues that should be addressed when MOFs are used in biomedical applications. For example, for a MOF to be considered as a potential drug carrier,[61] it must possess the following properties: non toxicity and bio-compatibility; high drug loading capacity; efficient delivery, control of release and matrix degradation.

For example, MIL-100 and MIL-101 have been loaded with anti inflammatory drug Ibuprofen into the pores and succeeded by loading of 0.35 g of Ibuprofen per gram of MIL-100 and 1.4 g of Ibuprofen per gram of MIL-101. Both MOFs were stable with the drug and complete guest release was achieved in approximately 3 days by MIL-100 and 6 days by MIL-101 into a simulated body fluid solution.[61]

REFERENCES

1.(a) Zhao, D.; Yuan, D.; Zhao, H. C. *Energy Environ, Sci*. **2008**, 1, 597. (b) Ferey, G. **2007**, 170A, 66. (c) Yaghi, O. M. *Nature Mater*. **2007**, 6, 92. (d) Roswell, J. L. C.; Yaghi, O. M. *Micropor Mesopor Mater*, **2004**, 73, 3.(e) Brammer, L. *Chem, Soc. Rev.* **2004**, 33, 476. (f) Braga, D. *Chem Commun*. **2003**, 2751. (g) James, S. L.; *Chem, Soc. Rev*. **2003**, 32, 276.(h) Janiak, C.; *Dalton Trans.* **2003**, 2781.(i) Rosi, N. L.; Eddaoudi, M.; Kim, J.; O'Keefe, M.; Yaghi, O. M.; *Cryst Eng Comm*, **2002**, 4, 401.

2) Hartmann, M.; Kevan, L. *Chem. Rev*. 99, **1999**, 635.

3) Davis, M. E. *Nature.* **2002**, 417, 813.

4) Inagaki, S.; Fukushima, Y.; Kuroda, K. J. *Chem. Soc. Chem. Comm*. **1993**, 680.

5) Imhof, A.; Pine, D. J. *Nature.* **1997**, 389, 948.

6) Stucky, G. D.; MacDougall, J.E. *Science.* **1990**, 247, 669.

7) Terasaki, O. *Solid State Phys*. **1992**, 27, 601.

8) Cox, S. D.; Dier, T. E.; Stucky, G. D.; Bierlein. *J. Am. Chem. Soc*. **1988**, 110, 2986.

9) Herron, N. *Am. Chem. Soc*. **1989**, 111, 530.

10) Vietze, U.; Krau, O.; Laeri, F.; *Phys Rev Lett*. **1998**, 81, 4628.

11) Wada, Y. *Am. Chem. Soc*. **2000**, 122, 8583.

12) Nozue, Y.; Kodaira, T.; Goto, T. *Phys. Rev. Lett*. **1992**, 68, 3789.

13) Simon, U.; Franke, M. E. *Micropor Mesopor Mater*. **2000**, 41, 1.

14) Davis, M.E.; Lobo, R.F. *Chem. Mater*. **1992**, 4, 756.

15) Baerlocher, C.; Meier, W. M.; Olson, D. H. *Elsevier*, 5th Ed, Amsterdam, **2001**.

16) James, S.L. *Chem Soc Rev*. **2003**, 32, 276.

17) Jagadeswara, R.K.; Krista, S.W. *Langmuir*. **2008**, 24, 16.

18) Kresge, C. T.; Leonowicz, M. E.; Roth, W. J.; Vartuli, J. C.; Beck, J. S. *Nature.* **1992**, 359, 710.

19) Oliver, S.; Kuperman, A.; Coombs, N.; Lough, A.; Ozin, G. A. *Nature.* **1995**, 378, 47.

20) Froba, M.; Tiemann, M. *Chem. Mater*. **1998**, 10, 3475.

21) Khimyak, Y. Z.; Klinowski, J. *Chem. Mater*. **1998**, 10, 2258.

22) Kimura, T.; Sugahara, Y.; Kuroda, K. *Chem. Mater*. **1999**, 11, 508.

23) Tiemann, M.; Froba, M.; Rapp, G.; Funari, S. S. *Chem. Mater.* **2000**, 12, 1342.

24) Kraushaarczarnetzki, B.; Stork, W. H. J.; Dogterom, R. *J. Inorg Chem.* **1993**, 32, 5029.

25) Gao, Q. M.; Xu, R.; Chen, J. S.; Li, R. S.; Li, S. G.; Qiu, S. L.; Yue, Y. J *Chem. Soc Dalton.* **1996**, 3303.

26) Snurr, R.Q.; Hupp, J.T.; Nguyen, S.T. *AICHE J.* **2004**, 50, 1090; Rowsell, J. L.C.; Yaghi, O.M. *Microporous Mesoporous Mater.* **2004**, 73, 3; Kitagawa, S.; Kitaura, R.; Noro, S. *Angew. Chem. Int.Ed.* **2004**, 43, 2334; Mueller, U.; Schubert, M.; Teich, F.; Puetter, H.; Schierle-Arndt, K.; Pastre, J. *J. Mater. Chem.* **2006**, 16, 626; Ferey, G.; *Chem. Soc. Rev.* **2008**, 37, 191.

27) Bae, Y.S.; Farha, O.K.; Hupp, J.T.; Snurr, R.Q. *J. Mater. Chem.* **2009**, 19, 2131.

28) Garcia-Perez, E.; Gascon, J.; Morales-Flores, V.; Castillo, J. M.; Kapteijn, F.; Calero, S. *Langmuir.* **2009**, 25 (3), 1725.

29) Banerjee, D.; Parise, J.B. *Cryst.Growth Des.* **2011**, 11, 4704.

30) Lee, J. D. *Concise Inorganic Chemistry*, Chapman & Hall, New York, **1991**.

31) Kim, M. K.; Jo, V.; Lee, D. W.; Shim, I. W.; Ok, K. M. *Cryst. Eng. Comm.* **2010**, 12, 1481.

32) Duan, X. Y.; Lin, J. G.; Li, Y. Z.; Zhu, C. J.; Meng, Q. J. *Cryst. Eng. Comm.* **2008**, 10, 207.

33) Williams, C. A.; Blake, A. J.; Wilson, C.; Hubberstey, P.; Schroeder, M. *Cryst. Growth. Des.* **2008**, 8, 911.

34) Volkringer, C.; Marrot, J.; Ferey, G.; Loiseau, T. *Cryst. Growth. Des.* **2008**, 8, 685.

35) Nguyen, T. L. A.; Demir-Cakan, R.; Devic, T.; Morcrette, M.; Ahnfeldt, T.; Auban-Senzier, P.; Stock, N.; Goncalves, A. M.; Filinchuk, Y.; Tarascon, J. M.; Ferey, G. *Inorg. Chem.* **2010**, 49, 7135.

36) Prestipino, C.; Regli, L.; Vitillo, J. G.; Bonino, F.; Damin, A.; Lamberti, C.; Zecchina, A.; Solari, P. L.; Kongshaug, K. O.; Bordiga, S. *Chem. Mater.* **2006**,18,1337.

37) Chen, B. L.; Eddaoudi, M.; Reineke, T. M.; Kampf, J. W.; O'Keeffe, M.; Yaghi, O. M. *J. Am. Chem. Soc.* **2000**, 122, 11559.

38) Vimont, A.; Goupil, J. M.; Lavalley, J. C.; Daturi, M.; Surble, S.; Serre, C.; Millange, F.; Ferey, G.; Audebrand, N. *J. Am. Chem. Soc.* **2006**, 128, 3218.

39) Forster, P. M.; Eckert, J.; Heiken, B. D.; Parise, J. B.; Yoon, J. W.; Jhung, S. H.; Chang, J. S.; Cheetham, A. K. *J. Am. Chem. Soc*. **2006**, 128, 16846.

40) Zou, R. Q.; Sakurai, H.; Han, S.; Zhong, R. Q.; Xu, Q. *J. Am. Chem. Soc*. **2007**, 129, 8402.

41) Chen, B. L.; Ockwig, N. W.; Millward, A. R.; Contreras, D. S.; Yaghi, O. M. *Angew. Chem. Int. Ed.* **2005**, 44, 4745.

42) Dinca, M.; Dailly, A.; Liu, Y.; Brown, C. M.; Neumann, D. A.; Long, J. R. *J. Am. Chem. Soc.* **2006**, 128, 16876.

43) Farha, O. K.; Spokoyny, A. M.; Mulfort, K. L.; Hawthorne, M. F.; Mirkin, C. A.; Hupp, J. T. *J. Am. Chem. Soc*. **2007**, 129, 12680.

44) Xiao, B.; Wheatley, P. S.; Zhao, X. B.; Fletcher, A. J.; Fox, S.; Rossi, A. G.; Megson, I. L.; Bordiga, S.; Regli, L.; Thomas, K. M.; Morris, R. E. *J. Am. Chem. Soc*. **2007**, 129, 1203.

45) Bae, Y. S.; Farha, O. K.; Spokoyny, A. M.; Mirkin, C. A.; Hupp, J. T.; Snurr, R. Q. *Chem. Commun*. **2008**, 35, 4135.

46) Alaerts, L.; Seguin, E.; Poelman, H.; Thibault-Starzyk, F.; Jacobs, P. A.; De Vos, D. E. *J. Chem. sEur*. **2006**, 12, 7353.

47) Horcajada, P.; Surble, S.; Hong, D. Y.; Seo, Y. K.; Chang, J. S.; Margiolaki, I.; Ferey, G. *Chem. Commun*. **2007**, 2820.

48) Surble, S.; Millange, F.; Serre, C.; Duren, T.; Latroche, M.; Bourrelly, S.; Llewellyn, P. L.; Ferey, G. *J. Am. Chem. Soc*. **2006**, 128, 14889.

49) Alexander, U. C.; Natalia, T.; Ulrich, M. *Chem. Soc. Rev*. **2009**, 38, 1284.

50) Mueller, U.; Schubert, M.; Teich, F.; Puetter, H.; Schierle-Arndt, K.; Pastre, J. *J. Mater. Chem.* **2006**, 16, 626.

51) (a) Zuttel, A.; *Naturwissenschaften*. **2004**, 91, 157. (b) Seayad, A. M.; Antonelli, D. M. *Adv. Mater*. **2004**, 16, 765. (c) Sakintuna, B.; Lamari-Darkrim, F.; Hirscher, M. *Int. J. Hydrogen Energy*. **2007**, 32, 1121.(d) Orimo, S.I.; Nakamori, Y.; Eliseo, J.R.; Zuttel, A.; Jensen, C. M. *Chem. Rev*. **2007**, 107, 4111.(e) Felderhoff, M.; Weidenthaler, C.W.; von Helmolt, R.; Eberle, U. *Phys. Chem. Chem. Phys.* **2007**, 9, 2643.

52) Yaghi, O. M.; Rowsell, J. L. C. *Angew. Chem. Int. Ed*. **2005**, 44, 4670.

53) Wicke, B. presentation for the Hydrogen Storage Materials Workshop, United States Department of Energy, Argonne, IL, August 14 – 15, **2002**.
54) Stern, A. C.; Belof, J. L.; Eddaoudi, M.; Space, B. Abstr Pap *Am. Chem. Soc*. **2007**, 233.
55) (a) Rowsell, J. L. C.; Millward, A. R.; Park, K. S.; Yaghi, O. M. *J Am. Chem. Soc.* **2004**, 126, 5666.(b) Panella, B.; Hirscher, M.; Putter, H.; Muller, U. *Adv. Funct. Mater*. **2006**, 16, 520.
56) Karger, B. L.; Snyder, L. R.; Horvath, C. An introduction to separation science, *Wiley*, New York, **1973**.
57) Mueller, U.; Hesse, M.; Puetter, H.; Schubert, M.; Mirsch, D. *Patent*, EP 1, **2005**, 674, 555,.
58) Mueller, U.; Hesse, M.; Puetter, H.; Kamieth, M.; Schierle, A. *Patent*, WO 2006072573 A2, **2006**.
59) Li, J. R.; Kuppler, R. J.; Zhou, H. C. *Chem. Soc. Rev*. **2009**, 38, 1477.
60) Mueller, U.; Schubert, M.; Teich, F.; Puetter, H.; Schierle-Arndt, K.; Pastre, J. *J Mater Chem*. **2006**, 16, 626.
61) Horcajada, P.; Chalati, T.; Serre, C.; Gillet, B.; Sebrie, C.; Baati, T.; Eubank, J. F.; Heurtaux, D.; Clayette, P.; Kreuz, C.; Chang, J. S.; Hwang, Y. K.; Marsaud, V.; Bories, P. N.; Cynober, L.; Gil, S.; Ferey, G.; Couvreur, P.; Gref, R. *Nat. Mater.* **2010**, 9, 172.
62) Pan, L.; Parker, B.; Huang, X.; Olson, D. H.; Lee, J. Y.; Li, J. *J. Am. Chem. Soc*. **2006**, 128, 4180.
63) Pan, L.; Olson, D. H.; Ciemnolonski, L. R.; Heddy, R.; Li, J. *Angew. Chem. Int. Ed.* **2006**, 45, 616.

Chapter 3

Methods and Instruments

1. Introduction

The hydro/solvothermal method was used for the synthesis of new compounds in this project. These new compounds were characterized using the following techniques: X-ray diffraction, Thermo gravimetric analysis, Infrared spectroscopy, UV-visible spectroscopy, and Fluorescence Spectroscopy.

2. Hydro/solvothermal methods

Hydrothermal synthesis can be defined as a method of synthesis of single crystals and different chemical compounds that depends on the solubility of minerals in hot water under pressure over 1 atm. The crystal growth is performed in an apparatus consisting of a steel pressure vessel called autoclave. These vessels are made of thick-walled steel

a)  b) 

Figure 3.1. (a) The parts of the autoclaves, (b) the entire setup the autoclave

materials which must withstand high temperatures and pressures for long period of time. As different solutions are used for synthesis, to prevent corrosion of the internal cavity of the autoclave, protective inserts are generally used. In this research only Teflon liners are used. The samples are placed first in the Teflon bags, then these bags are kept in Teflon liner and closed with a cap on the top, then this cup is placed into the autoclave. The autoclave is closed tightly. The parts of the autoclaves are shown in the Figure 3.1.

3. Powder X-Ray Diffraction

X-ray Diffraction is a non-destructive analytical technique which reveals information about the crystal structure, chemical composition, and physical properties of materials and thin films. These techniques are based on observing the scattered intensity of an X-ray beam hitting a sample as a function of incident and scattered angle, polarization, and wavelength or energy.

Each crystalline solid has its unique characteristic X-ray powder pattern which may be used as a "fingerprint" for its identification. Once the material has been identified, X-ray crystallography may be used to determine its structure.

X-ray powder diffraction is a rapid analytical technique primarily used for phase identification of a crystalline material and can provide information on unit cell dimensions. The analyzed material is finely ground, homogenized, and average bulk composition is determined.

Instrument and Method

The instrument used for Powder X-Ray Diffraction in my project is ARL Thermo X-ray Diffractometer. Thermo ARL is the name of the company which designed this instrument. The purity and the stability of the samples were analyzed using this instrument. The powder samples were analyzed using ARL Thermo X-ray Diffractometer measurements. The sample was swept from $2\theta = 2^{\circ}$ to 60° with a speed of 1.2°/minute. The X-ray generator was set to 20 kV and 20 mA.

After the samples were analyzed the purity and the stability can be determined by comparing sample pattern with simulated pattern. The picture of the ARL Thermo X-ray Diffractometer is shown in Figure 3.2.

Figure 3.2. ARL Thermo X-ray Diffractometer

4. Single crystal X-Ray Diffraction

Single crystal X-ray diffraction is a non-destructive analytical technique which provides detailed information to facilitate the determination of the structure of a material. The information collected includes; crystal symmetry, unit cell dimensions, details of site-ordering, atomic positions and space group. These unit cell parameters can be used to verify if a structure is new or known in the literature by comparing this data with online databases.[1, 2, 3]

Single crystal X-ray diffraction is based on inference of monochromatic X-rays and a crystalline sample. These X-rays are generated by a cathode ray tube, filtered to produce monochromatic radiation, collimated to concentrate, and directed toward the sample. The interaction of the incident rays with the sample produces constructive interference (and a diffracted ray) when conditions satisfy Bragg's Law ($n\lambda=2d\sin\theta$). This law relates the wavelength of electromagnetic radiation to the diffraction angle and the lattice spacing in a crystalline sample. These diffracted X-rays are then detected, processed and counted. By changing the geometry of the incident rays, the orientation of the centered crystal and the detector, all possible diffraction directions of the lattice can be attained.

Instrument and Method

The instrument used for Single crystal X-Ray Diffraction in my project is Bruker Quazar diffractometer. X-ray diffraction data for different were collected on a Bruker Quazar diffractometer with an Apex II CCD area detector. The data was processed with the SAINT software[4] and corrected for absorption with SAD-ABS.[5] The structures was

Figure 3.3. Bruker Quazar diffractometer

solved by direct methods SHELXTL V.6.10 package[6] and was refined against F2 by weighted full-matrix least-squares calculations.[7] All non-hydrogen atoms were refined allowing for anisotropic displacement. Hydrogen atoms were localized from the difference Fourier maps. Atomic scattering factors were taken from the International Tables for Crystallography.[8]

5. Thermo Gravimetric Analysis

Thermo gravimetric analysis (TGA) is a technique performed on samples to determine changes in weight in relation to change in temperature. It provides a quantitative measurement of the mass changes in a material associated with both material transitions and thermal degradation and thus can be used in the determination of the thermal stability and decomposition products of a material. The instrument used for analysis is shown in figure 3.4.

Instrument and Method

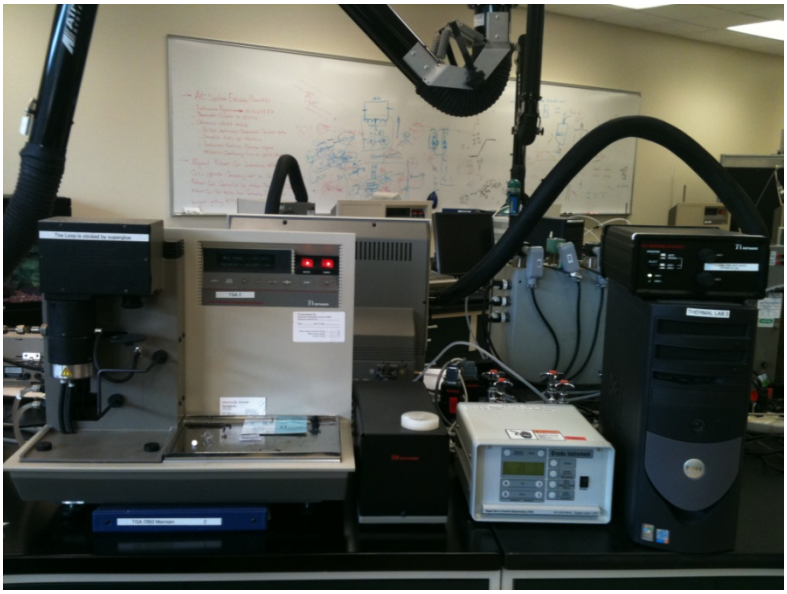

Figure 3.4. TA Q5000 Thermogravimetric Analyzer

The instrument used for the analysis of the thermal properties is TA Q 5000 Thermogravimetric Analyzer. The sample was isothermal for 5min and then heated from

30°C to 600°C with the heating rate of 10°C /min in an air atmosphere with flow rate of 35 mL/min.

6. Fluorescence Spectroscopy

Fluorescence spectra were obtained by a PerkinElmer LS55 fluorescence spectrophotometer. The principle of fluorescence is that when atoms are elevated to higher energy levels, they sometimes return to the ground state through a pathway, which has several intermediate electronic states, before reaching to the actual ground state. Such series of fall through the electronic levels accompany by light emission. This is called as fluorescence.

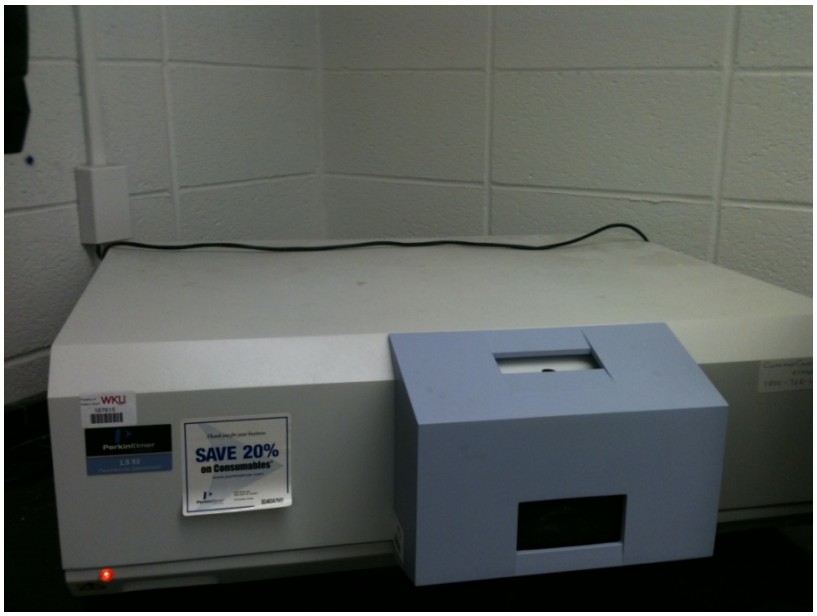

Figure 3.5. PerkinElmer LS55 fluorescence spectrophotometer.

7. UV-visible spectroscopy

Ultraviolet-visible (UV-vis) diffuse reflectance spectra (DRS) were obtained using a Varian Cary 100 UV-vis spectrophotometer equipped with the DRA-CA-30 diffuse reflectance accessory.

Figure 3.6. Cary 100 UV-vis spectrophotometer

8. Infrared Spectroscopy

The infrared spectra were recorded from 400 to 4000 cm-1 on a Perkin Elmer Spectrum One FTIR spectrometer using KBr pellets. The background scan was collected with KBr pellets.

Figure 3.7. Perkin Elmer Spectrum One FTIR spectrometer

9. Materials

The different chemicals used in this research project are purchased from different companies. The chemicals list is given in the Table 3.1

Table 3.1. Different chemical materials

Name of the chemical	Formula	Company Name	Grade
Benzene 1,3,5-tricarboxylic acid	$C_6H_3(CO_2H)_3$	Alfa Aesar	98%
Pyrazine 2 -carboxylic acid	$C_5H_4N_2O_2$	Alfa Aesar	99%
Calcium chloride	$CaCl_2$	Alfa Aesar	96%
Magnesium nitrate	$Mg(NO_3)_2$	Fischer Sceintific	98+%
Calcium nitrate hexahydrate	$Ca(NO_3)_2{\cdot}6H_2O$	Fischer Sceintific	Technical
Benezene 1,4-dicarboxylic acid	C_6H_4 1-4-$(CO_2H)_2$	Alfa Aesar	98+%
Ethylenediamine	$NH_2CH_2CH_2NH_2$	Fischer Sceinticfic	certified
Dimethyl formamide	$HCON(CH_3)_2$	Alfa Aesar	99.8%
Rubidium Hydroxide	RbOH	Alfa Aesar	50%w/w aqu
Hydrochloric acid	HCl	Sigmaalrich	ACS
Sodium hydroxide	NaOH	Fischer Sceintific	Technical
4,5imidazole dicarboxylic acid	$C_5H_4N_2O_4$	Alfa Aesar	97%

REFERENCES

1) Bennett, D. W. Understanding single-crystal x-ray crystallography; *Wiley-VCH*: Weinheim, **2010**.

2) Clegg, W. Crystal structure determination; *Oxford University Press*: Oxford; New York, **1998**.

3) Fletcher, D. A.; McMeeking, R. F.; Parkin, D. *J Chem Inf Comp Sci*. **1996**, 36, 746.

4) Ellsworth, J. M.; zur Loye, H.-C. *Dalton Trans*. **2008**, 5823.

5) SAINT Frame Integration Software; Bruker AXS Inc. Madison, WI, **2000**.

6) G. M. Sheldrick, & SADABS, Siemens Area Detector Absorption (and other) Correction," Univ. of Gottinger, Gottinger, Germany, **1998**.

7) SHELXTL ver. 6.14, Reference Manual, Bruker Industrial Automation, Analytical Instrument, Madison, WI 53719, **2000**.

8) Sheldrick, G.M. *Acta Cryst*. **2008**, A64, 112.

9) Skoog, D. A.; Holler, F. J.; Crouch S.R. Principles of instrumental analysis, 6th edition, Brooks Cole, Dec 6**, 2006**.

Chapter 4

Synthesis and characterization of two- and three-dimensional calcium coordination polymers built with benzene-1, 3, 5-tricarboxylate and/or pyrazine-2-carboxylate

1. Introduction

Metal–organic framework (MOF) materials, which are also known as coordination polymers, have attracted extensive research studies[1] because of their potential applications in many areas, such as gas storage,[2] separations,[3] sensors[4] and heterogeneous catalysis.[5] The general approach of making these materials is usually the fabrication of metal ion building units and multidentate organic ligands in appropriate solvents under hydro/sovolthermal conditions. From the point view of coordination chemistry, the assembly of the building units into designed MOF structures is controlled by many parameters, such as the metal coordination geometry, the Lewis acidity of the metal, the Lewis basicity of the ligands, and the number and type of donor atoms and their orientations. In recent years, non-covalent interactions, such as hydrogen-bonding,[6] ionic interactions, and π-π stacking[7] between building units are also considered as important factors in the self-organization of the frameworks. Although it is impossible to exactly control all of these factors at the same time when designing a MOF, it is usually realistic to tune the combination of suitable metal ions and proper organic linkers in order to tailor structural geometries, connectivity, and subsequent properties, such as the adsorption of small molecules. In recent years, in addition to transition metals, main group metals have also been used to synthesize novel metal-organic network topologies.[8]

In contrast to the huge amount of MOFs built from transition metal ions reported in the literature,[1-5] there are a relatively limited number of examples based on the alkaline earth metals. However, a few studies on magnesium and calcium have been reported.[9] Recent reports show that doping alkaline earth metals[10] or alkaline metals[11] in MOFs may enhance their ability for gas storage due to the stronger binding capability of these metals to certain gases such as CO_2 or H_2. Moreover, the assembly of MOFs from calcium and polycarboxylate linkers, including aliphatic or aromatic carboxylates ligands, has been investigated and is receiving increasing interest.[12] Due to their flexibility as mono-, bi-, or multidentate ligands, carboxylic acids, such as btc and pzc,[13] have been investigated for the synthesis of coordination polymers with a diverse range of topologies and conformations. This project is the synthesis of porous materials and the study of their properties, such as their ability to absorb/remove mercury in flue gas of power plants. The approach is to develop novel materials based on alkaline earth MOFs to specifically recognize, bind, and capture mercury. In this chapter, the synthesis and structural characterization of two new crystalline alkaline earth metal coordination polymer phases, $[Ca_3(btc)_2(H_2O)_{12}]$ (**1**), and $[Ca_2(btc)(pzc)(H_2O)_3]$ (**2**) are reported. The thermal properties and luminescent behavior of these materials are also discussed.

2. Experimental section

Materials and Methods

Infrared spectroscopy

The infrared spectra were recorded from 400 to 4000 cm^{-1} on a Perkin Elmer Spectrum One FTIR spectrometer using KBr pellets.

Thermogravimetric Analysis

The thermogravimetric data were collected on a TA Q5000 TGA instrument at a heating rate of 10°C min^{-1} from room temperature to 800°C in an air atmosphere.

Powder X-ray Diffraction

Powder X-ray analysis was performed on an ARL Thermo X-ray Diffractometer using Cu Kα radiation (1.5418 Å), in which the X-ray tube was operated at 40 kV and 40 mA. The resulting crystal structure was used to simulate the powder pattern, which was found to have good agreement with the experimental data.

Fluorescence spectra

Fluorescence spectra were obtained by a PerkinElmer LS55 fluorescence spectrophotometer.

UV-vis spectrophotometer

Ultraviolet-visible (UV-vis) diffuse reflectance spectra (DRS) were obtained using a Varian Cary 100 UV-vis spectrophotometer equipped with the DRA-CA-30 diffuse reflectance accessory.

Compound $[Ca_3(btc)_2(H_2O)_{12}]$ (1)

Compound **1** was synthesized from a mixture of calcium chloride, benzene 1,3,5-tricarboxylic acid, ethylenediamine (en) and water. A typical synthesis is as follows: 1.0 mL of water containing 0.098 g of H_3btc were mixed with 1.0 mL aqueous solution of 0.217 g $CaCl_2$ and stirred. To the resulting mixture, 0.036 g of en aqueous solution (en: H_2O ratio, 1:2) was added and the mixture was stirred for 30 minutes using a magnetic stir bar. The pH of this mixture was adjusted with 2M NaOH to approximately 9.4. The reaction mixture was transferred to a Teflon bag, sealed and placed in a 45 mL reaction vessel, and heated in an oven at 180°C for 24 hours. Colorless crystals were filtered and dried in air for overnight (yield: 0.117 g). UV DRS (solid) 260 nm, 290 nm, 310 nm (shoulder).

Compound $[Ca_2(btc)(pzc)(H_2O)_3]$ (2)

Compound **2** was synthesized from a mixture of calcium nitrate hexahydrate, benzene 1,3,5-tricarboxylic acid, pyrazine-2-carboxylic acid, dimethylformide (DMF) and water. A typical synthesis is as follows: a mixture of 0.125 g btc and 0.072 g pzc in 1.0 mL of DMF was added to 1.0 mL aqueous solution containing 0.291 g of $Ca(NO_3)\cdot 6H_2O$. The resulting mixture was stirred for 30 minutes and the pH was then adjusted with 2M NaOH and to approximately pH 6.98. The reaction mixtures were transferred to a Teflon bag, sealed and placed in a 45 mL reaction vessel, and heated in an oven at 130°C for 24 hours. Colorless crystals were filtered and dried in air for overnight (yield: 0.113g UV DRS (solid) 250 nm, 275 nm and 310 nm (shoulder).

X-ray Crystallography

X-ray diffraction data for compounds **1** and **2** were collected on a Bruker Quazar diffractometer with an Apex II CCD area detector. The data was processed with the SAINT software[14] and corrected for absorption with SAD-ABS.[15] The structure was solved by direct methods SHELXTL V.6.10 package [16] and was refined against F^2 by weighted full-matrix least-squares calculations[17]. All non-hydrogen atoms were refined allowing for anisotropic displacement. Hydrogen atoms were localized from the difference Fourier maps. Atomic scattering factors were taken from the International Tables for Crystallography. [18] Crystal data and relevant details of the structure determinations are summarized in Table 4.1 and selected geometrical parameters are given in Table 4. 2.

3. Results and Discussion

The Structure description of compound 1

The structure of compound **1** is a three-dimensional framework consisting of Ca ions, btc ligands, and coordinated waters. As shown in Figure 4.1 a, its asymmetric unit consists of one and a half Ca atoms, two halves of btc ligands and six coordinated water molecules. Ca(1) binds to four water molecules and two carboxylate oxygens of two btc ligands (Figure 4.1 b). Ca(2) is eight-coordinated by four water molecules and four carboxylate oxygen atoms of two btc ligands (Figure 4.1c). The two btc ligands share the same coordination environment: coordinating to three Ca atoms with its three carboxylate groups (Figure 4.1 d). The Ca-O bond lengths are in the range of 2.299(1)-2.967(2) Å. Bond valence calculations gave a value of +2.07 for both Ca(1) and Ca(2) cations.[19]

Table 4.1. Crystal data and structure refinements for compounds **1** and **2**.

	1	2
Formula	$C_{18}H_{30}Ca_3O_{24}$	$C_{14}H_{12}Ca_2N_2O_{11}$
Mol. wt.	750.66	464.42
Crystal system	Monoclinic	Orthorhombic
Space group	*C*2/c	$P2_12_12_1$
a (Å)	6.7257(1)	8.9512(2)
b(Å)	20.8422(4)	12.9606(4)
c(Å)	20.1942(4)	14.4060(3)
α(°)	90	90
β(°)	99.507(1)	90
γ(°)	90	90
V(Å^3)	2791.91(9)	1671.28(7)
Z	4	4
ρ (Mg/m^3)	1.786	1.846
μ (mm^{-1})	0.699	0.753
Wavelength(Å)	0.71073	0.71073
Temperature(K)	296	296
Reflections collected/unique [R_{int}]	46626/0.0625	74114/0.112
Goodness-of-fit(F^2)	0.947	0.930
Final R indices [$I > 2\sigma(I)$]	R_1= 0.0408, wR_2= 0.1029	R_1= 0.0328, wR_2= 0.0606
R indices (all data)	R_1= 0.0625, wR_2= 0.1162	R_1= 0.0498, wR_2= 0.0648

Table 4. 2. Selected Bond Lengths [Å] for compounds **1** and **2**.

Compound 1		Compound 2	
Ca(1)-O(2)#1	2.299(1)	Ca(1)-O(4)#1	2.297(1)
Ca(1)-O(4W)	2.330(1)	Ca(1)-O(6)#2	2.411(1)
Ca(1)-O(5)#2	2.342(1)	Ca(1)-O(7)#2	2.413(1)
Ca(1)-O(1W)	2.398(1)	Ca(1)-O(2)	2.462(1)
Ca(1)-O(3W)	2.436(1)	Ca(1)-O(1W)	2.478(2)
Ca(1)-O(2W)	2.454(1)	Ca(1)-O(2W)	2.518(2)
Ca(1)-O(5W)	2.967(2)	Ca(1)-O(1)	2.586(1)
		Ca(1)-O(8)#2	2.771(2)
Ca(2)-O(6W)#3	2.335(2)	Ca(2)-O(3)#3	2.300(1)
Ca(2)-O(6W)	2.335(2)	Ca(2)-O(1)	2.322(1)
Ca(2)-O(4)#3	2.490(1)	Ca(2)-O(3W)	2.366(2)
Ca(2)-O(4)	2.490(1)	Ca(2)-O(7)	2.394(1)
Ca(2)-O(5W)#3	2.539(2)	Ca(2)-O(5)#2	2.396(2)
Ca(2)-O(5W)	2.539(2)	Ca(2)-O(6)#2	2.552(2)
Ca(2)-O(3)	2.543(1)	Ca(2)-N(1)	2.596(2)
#1 -x+2,-y+2,-z; #2 -x+3/2,-y+3/2,-z; #3 -x+2,y,-z+1/2		#1 -x+3/2,-y,z-1/2; #2 -x+1/2,-y,z-1/2; #3 x-1,y,z	

Ca(1) atoms forms a helical chain (Figure 4.2 a) along the *a* direction, with adjacent Ca

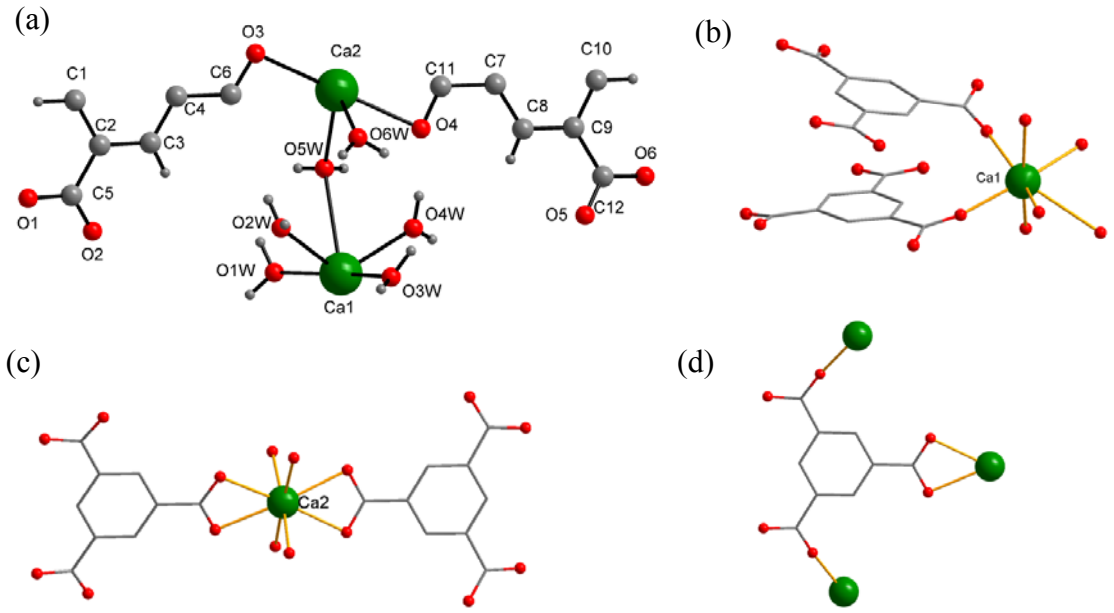

Figure 4.1. (a) The asymmetric unit; (b) the coordination environment of Ca (1); (c) the coordination environment of Ca(2); and (d) the coordination environment of btc in compound **1**.

atoms linked through two carboxylate oxygens of a btc ligand. In the chain, the Ca(1) atoms line up in two parallel columns along the *a* axis with the nearest Ca(1)…Ca(1) distance of 6.726 Å. Hydrogen bonds form along the column between water molecules from neighboring Ca(1) atoms (O(3W)-H…O(1W): 2.943 Å). The neighboring Ca(1) atoms from different columns are linked by btc ligands to form the helical chain. The dihedral angle between neighboring benzene rings is calculated as 11.83(6)°, and C…C distances in the range 3.08-3.57 Å, indicating π-π interactions between aromatic rings. The structure of **1** contains both left- and right-handed helical chains, hence the crystal is achiral. The third carboxylate of each linking btc ligand is pointing towards the opposite

direction of its neighboring btc ligands in the helical chain, and coordinates to Ca(2) cations, which link the helical chains of same handness into a chiral layer parallel to the *ab* plane (Figure 4.2b). Neighboring chains in the layer are related by shifting a half unit along the a axis, and neighboring layers contain chains of different handness.

Each Ca(1) cation in a layer is sharing two water molecules with Ca(2) from the adjacent layers (Ca(1)-O, 2.967(2); Ca(2)-O, 2.539(2) Å), forming a three-

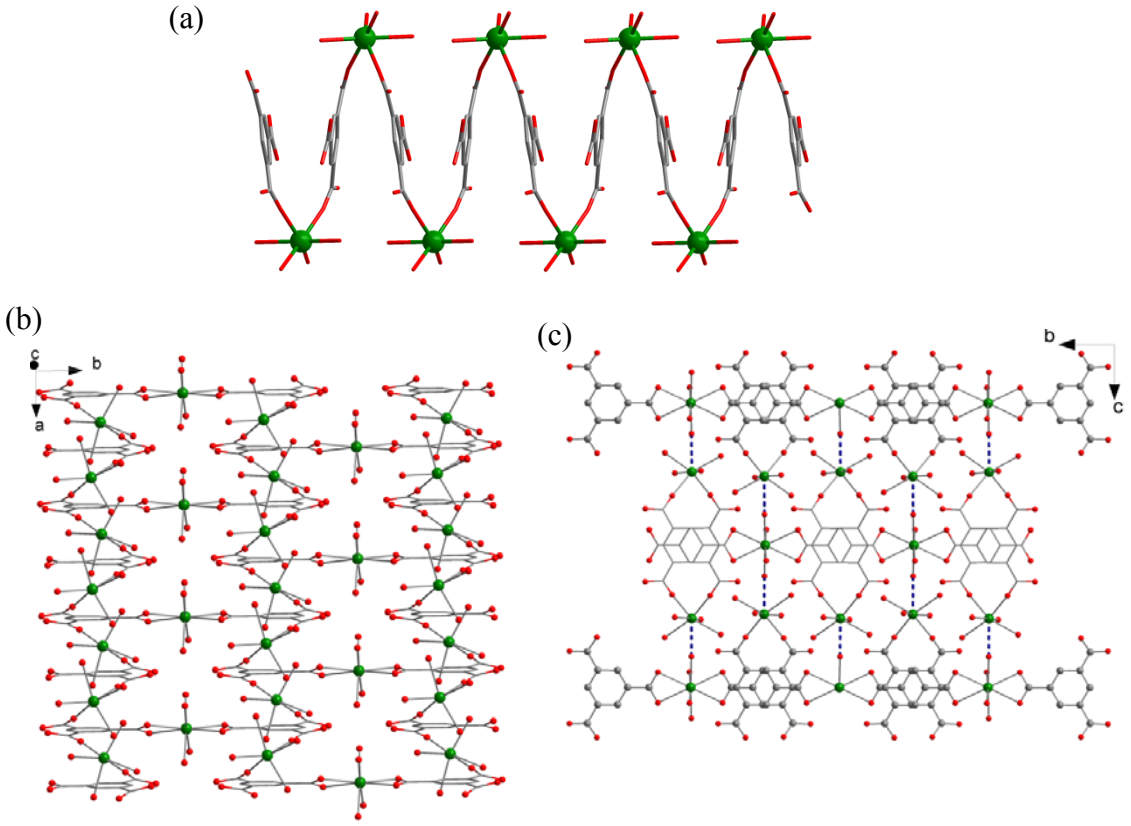

Figure 4.2. (a) The helical chain in compound **1**; (b) the layer in **1** formed by helical chains linked through Ca(2); (c) the 3D structure of **1** formed by bridging water molecules between neighboring layers.

dimensional framework (Figure 4.2 c), in which the layers are stacked along the *c* direction in an ABAB… manner. Thus, Ca(1) connects to four unshared waters while Ca(2) binds to two unshared waters. These waters point to voids formed by the framework of **1** and can be potentially removed to form open metal sites on Ca ions.

To date, only three calcium/btc based coordination polymers $[Ca_3(btc)_2(H_2O)_{12}]$ (**3**),[12b] $[Ca(Hbtc)(H_2O)_2]$ (**4**),[6b] $[Ca_3(btc)_2(DMF)_2(H_2O)_2]_3 \cdot 3H_2O$ (**5**),[12j] have been reported. Compounds **3** and **4** are layered structures, while **5** is a 3D framework. Compound **1** represents the second 3D framework constructed from btc and calcium building units.

Structure Description of Compound 2

The structure of compound **2** is a double layered network. As shown in Figure 4.3 a, the asymmetric unit of **2** consists of two unique calcium ions, one btc, one pzc, and three coordinated water molecules. Ca(1) is eight-coordinated to six carboxylate oxygens of three btc and one pzc ligands, and two water molecules (Figure 4.3 b), while Ca(2) is seven-coordinated to five carboxylate oxygens of btc/pzc ligand, one nitrogen of pzc, and one oxygen of water (Figure 4.3 c). The btc ligand is connected to six calcium ions using its three carboxylate groups. The pzc ligand binds to two Ca ions via its two O atoms and one N atom, leaving one N atom uncoordinated (Figure 4.3 d). The Ca-O distances are 2.297(1)-2.771(1) Å and Ca-N is 2.596(2) Å. Bond valence calculations gave a value of +2.05 for Ca(1) and 2.23 for Ca(2).

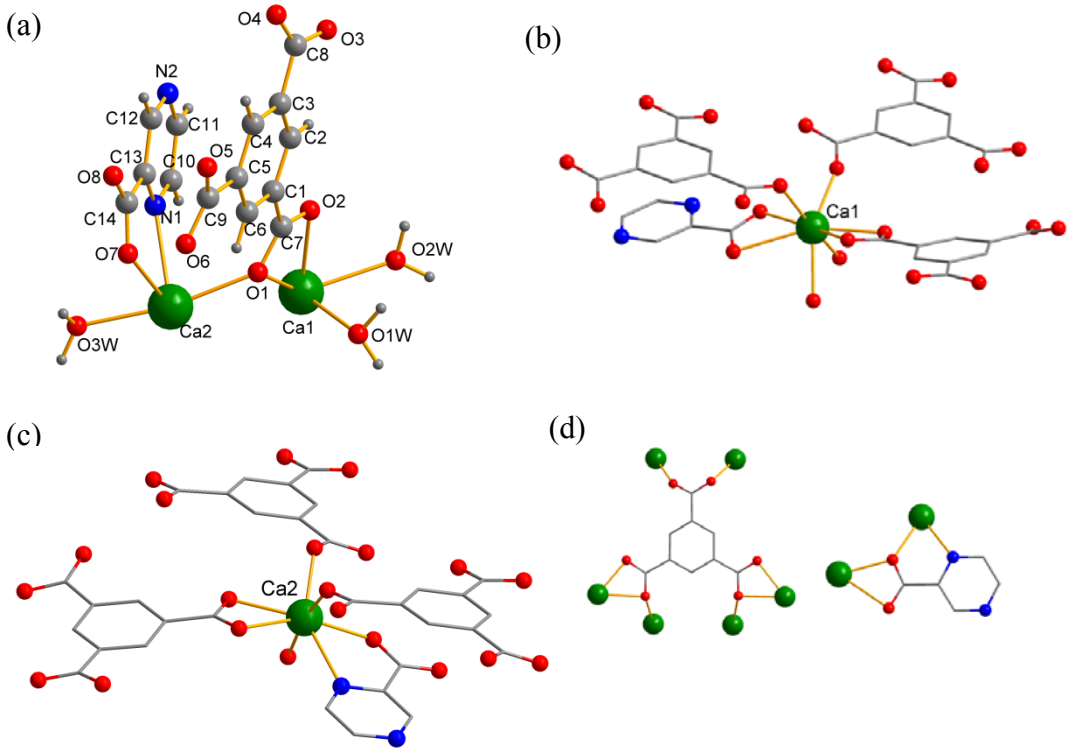

Figure 4.3. (a) The asymmetric unit; (b) the coordination environment of Ca(1); (c) the coordination environment of Ca(2); and (d) the coordination environment of btc and pzc in compound **2**.

The Ca(1) ion is sharing two oxygen atoms with Ca(2) ion to form a dimer unit

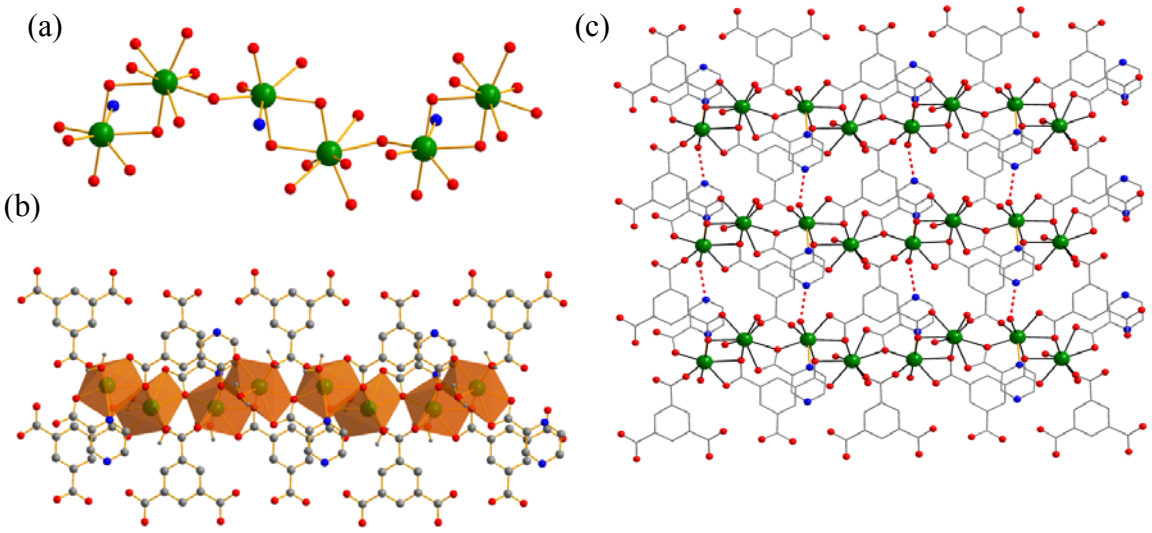

Figure 4.4. (a) The zigzag chain in compound **2**; (b) The zigzag chain with ligands in compound **2**; (c) the 2D structure of **2** formed by bridging btc ligands between neighboring layers (hydrogen bonds are shown in dash lines).

$\{Ca_2O_{12}N\}$, which in turn is connected to two neighboring dimers into a zigzag chain by corner sharing the oxygen atoms (Figure 4.4 a). These chains then form a layered structure by sharing btc ligands between neighboring chains. An interesting feature of **2** is that only one of the two pzc nitrogen atoms coordinates to a calcium ion. The other nitrogen atom of pzc from one chain forms strong hydrogen bonds (O(3W)···N(2), 2.809(2) Å) to water molecules on the adjacent chains. This provides additional force in the assembly of inorganic chains to adopt a layered structure (Figure 4.4c). Strong hydrogen bonds (O(1W)···O(2), 2.709(2) Å; O(2W)···O(3), 2.774(2) Å) also formed between layers to hold the layers into a 3D network.

Although there are many coordination polymers containing the pzc ligand,[13] to the best of our knowledge, no Ca/pzc based MOF have been reported so far. Ptasiewicz-Bak *et al.* reported a monomeric calcium complex based on pzc ligand $[Ca(pzc)_2(H_2O)_4]$.[20] Therefore, compound **2** represents the first pzc based Ca coordination polymer synthesized from hydrothermal reactions.

Powder X-Ray Diffraction

The purity of the products was determined by powder X-ray diffraction (PXRD) measurements. The powder X-ray diffraction for compound **1** was shown in Figure 4.5. The agreements between simulated and experimental patterns proved that the product compound **1** is pure and does not contain any impurities.

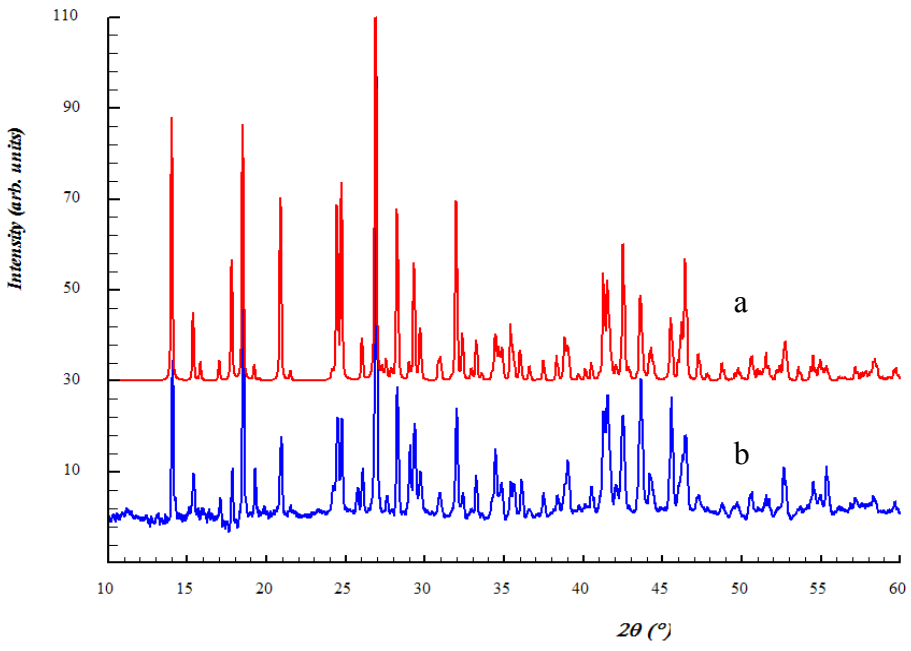

Figure 4.5. Simulated (a) and Experimental (b) powder X-ray patterns of compound **1**.

The purity of the products was determined by powder X-ray diffraction (PXRD) measurements .The powder X-ray diffraction for compound **2** was shown in Figure 4.6. The agreements between simulated and experimental patterns proved that the product compound **2** is pure and does not contain any impurities.

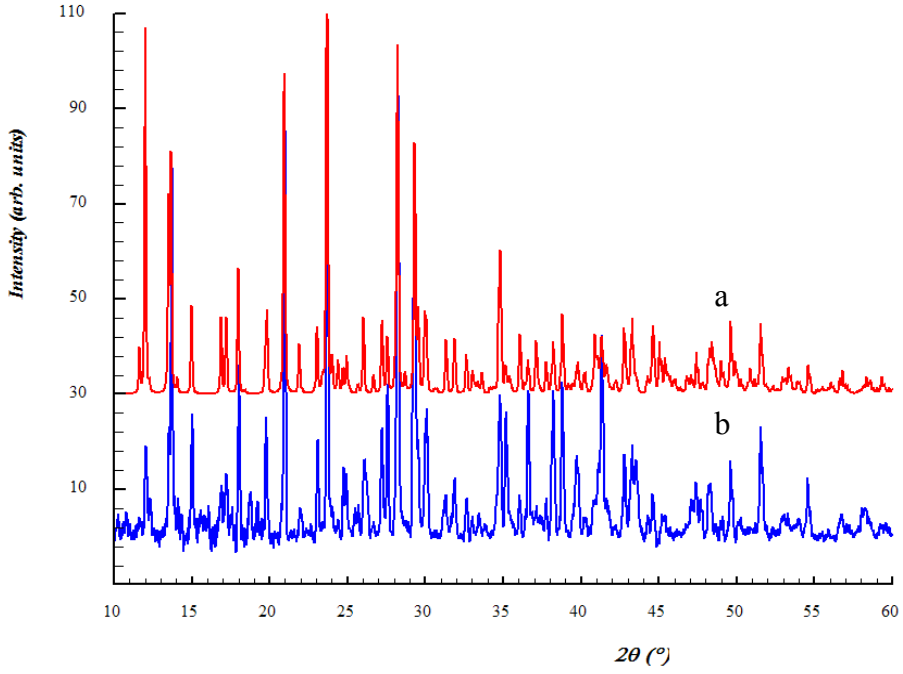

Figure 4.6. Simulated (a) and Experimental (b) powder X-ray patterns of compound **2**.

Thermogravimetric Analysis

To study the thermal stability, a thermogravimetric analysis was performed on

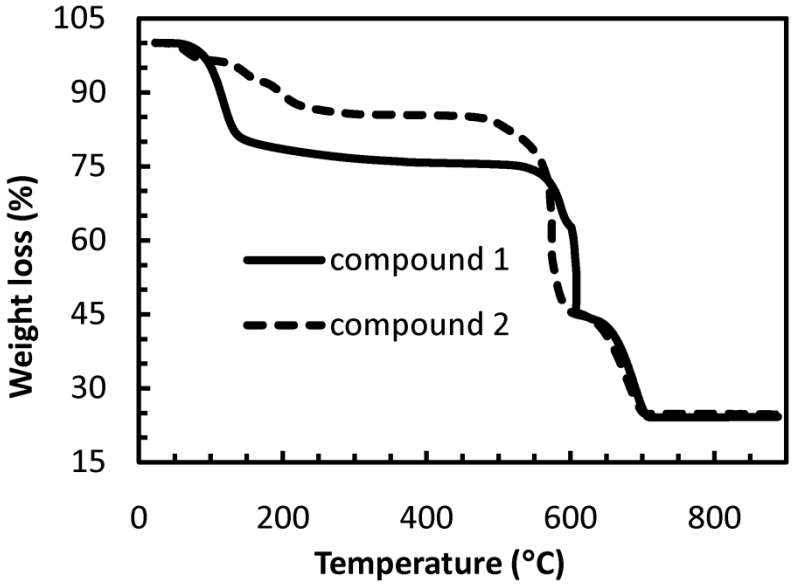

Figure 4.7. Thermogravimetric analyses of compounds **1** and **2**.

both compounds **1** and **2** (Figure 4.7). Crystalline samples were heated from 30 to 900°C in air at a heating rate of 10°C/min. An initial weight loss of approximately 19.0% over a temperature range of 40-140°C was observed for compound **1**. This could be attributed to the loss of eight coordinated water molecules per formula unit (calculated 19.2%). In the range of 140-350°C, a further loss of 4.9% (calc 4.8%) could be the loss of two water molecules per formula unit. The weight loss of 51.1% (520-700°C, clc 50.9%) is attributed to the removal and decomposition of the btc ligand and the formation of calcium oxide.

As for compound **2**, the weight loss of 11.9% in three steps over the range of 40-225°C corresponds to the removal of three water molecules (calc. 11.6%), and all coordinated waters are removed at this stage. In the 450-700°C range, a weight loss of

61.2% is observed in two steps. This is caused by the decomposition and removal of pzc and btc ligands (calc. 64.2%).

UV-vis Spectroscopy

The UV-vis spectra of both ligands in aqueous solution and solid samples have been recorded and are presented in Figures 4.8-4.11. The UV-vis spectra of free Hpzc ligand in aqueous solution exhibits three bands at 205, 268, and 312 nm. The two strong bands at higher energy level are assigned to π-π* transitions and the weak band to n-π* transition. The strong π-π* transition band of free H_3btc ligand in aqueous solution is located at 209 nm with a shoulder at 238 nm. The n-π* transition band at ~ 294 nm of free H_3btc ligand is very weak. The transition band positions of the solid free ligand samples in their UV-vis diffuse reflectance spectra are rather different from the solution absorption spectra. The DRS of pzc shows two broad bands at 250 nm (shoulder at 210 nm) and 315 nm. The btc ligand has two bands at 250 nm (shoulder at 210 nm) and 285 nm. The bands at lower energy can be assigned to the n-π* transition, which is stronger in solid state samples.

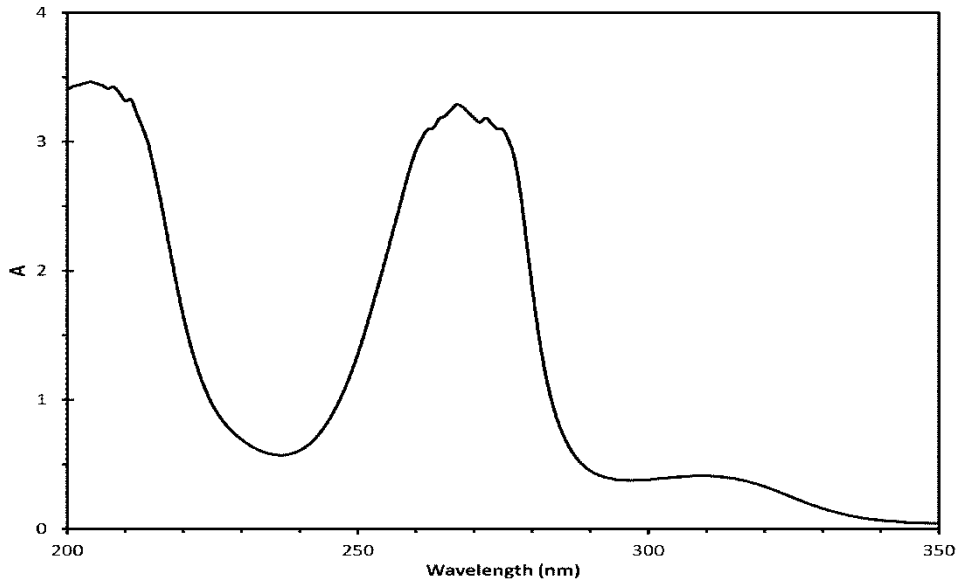

Figure 4.8. UV-vis spectra of free Hpzc ligand in aqueous solution

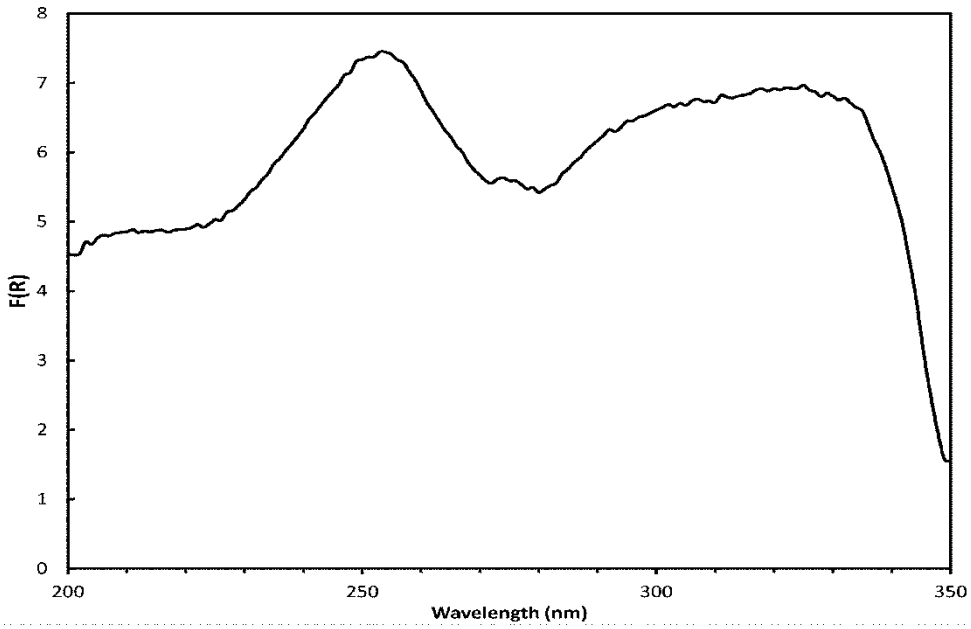

Figure 4.9. UV-vis Diffuse reflectance spectra of Hpzc

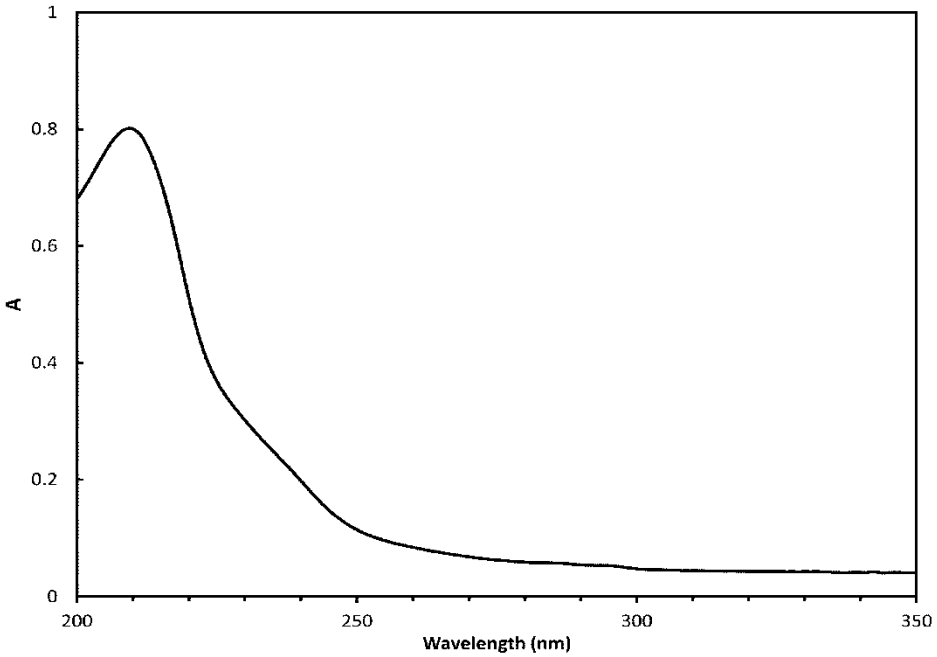

Figure 4.10. UV-vis spectra of H_3btc in aqueous solution

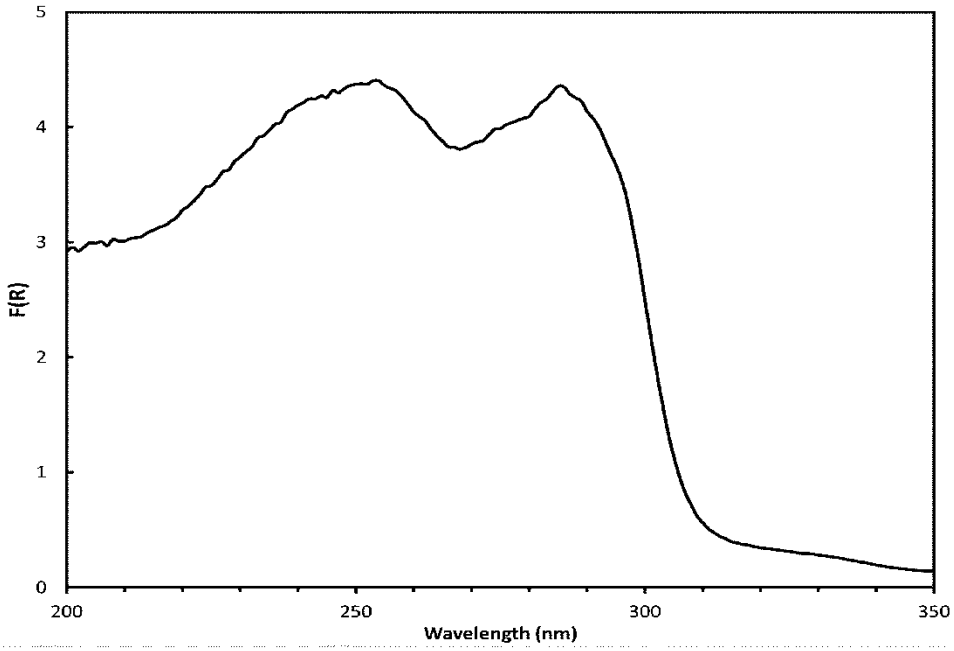

Figure 4.11. UV-vis Diffuse reflectance spectra of H_3btc

As shown in Figure 4.12, when the btc ligand coordinates to Ca^{2+} in compound **1**, the transition bands of UV-vis DRS shifted slightly to lower energy in comparison with

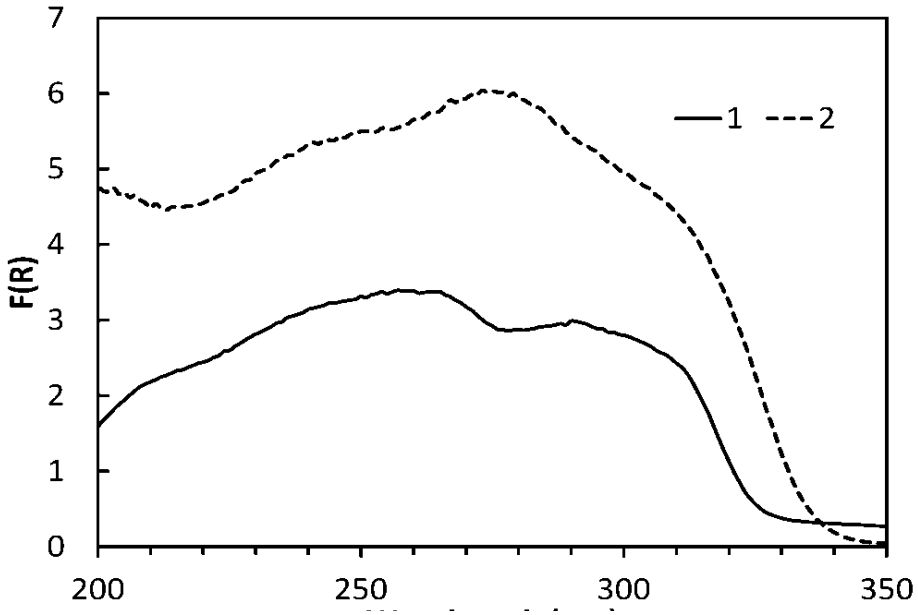

Figure 4.12. UV Diffuse reflectance spectra of compounds **1** and **2**

free btc ligands. The UV-vis DRS of **2** are complicated due to the presence of two organic ligands. The strongest band is at λ_{max} = 275 nm, which can be attributed to n-π* transition.

Fluorescent Emissions

The fluorescent spectra of compounds **1** and **2** as solid suspensions in water were studied at room temperature and their emission spectra are depicted in Figure 4.13. The only organic ligand in compound **1** is btc, whose free form (H_3btc), when excited at

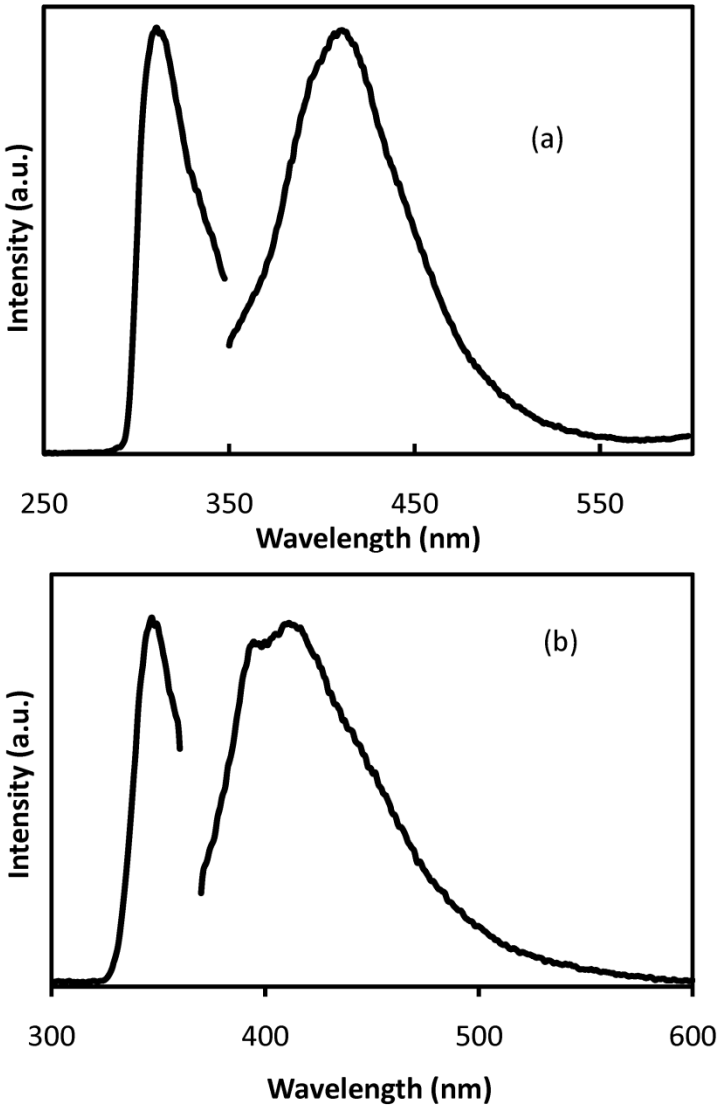

Figure 4.13. The excitation-emission spectra of (a) compound **1** and (b) compound **2** at room temperature.

334 nm, shows the emission at λ_{max} = 370 nm, which can be assigned to the π^*-*n* transition (Figure 4.13.1).[21] The emission spectrum of **1** shows a peak at 406 nm when excited at 308 nm. The hypsochromic shift of the excitation in **1** (from 334 to 308 nm) could possibly be explained by a change of the *n* orbital energy level on oxygen atoms due to the coordination of Ca^{2+} and the hydrogen bonding to the carboxylate oxo groups. The π^* orbitals, however, might be slightly affected due to the twisting of the btc ligand away from the coplanar form (the dihedral angles between the carboxylate groups and the benzene aromatic ring: *ca*. 12.53°, 7.83°, 3.3°, 15.9° for C(5), C(6), C(11), C(12), respectively). It is not clear why emission of **1** show a hypochromic shift. However, it has been suggested in the presence of a cation that strongly interacts with the lone pair of the carbonyl group, the n-π^* state is likely to be shifted to higher energy so that the lowest excited state becomes π-π^* transition.[22] Thus, it is possible that the emission in **1** is from a low lying π^*-π transition. Similar to other reported Ca coordination polymers,[12j] it is reasonable to assume in **1** that the emission is essentially a ligand centered transition.

Compound **2** contains mixed organic ligands of btc and pzc. The free ligand of Hpzc exhibits similar emission (λ_{ex} = 357 and λ_{em} = 427 nm, Figure 4.13.2) to free btc ligand. Upon excitation at 347 nm, the luminescence spectra of compound **2** exhibit two emissions: 394 and 410 nm, which is originated from btc and pzc respectively. The excitation of **2** slightly blue-shifted when compared with the free pzc ligand, and this is likely due to the coordination of N to Ca ions in **2**. The two emission peaks in **2** can be attributed to ligand-centered transitions.

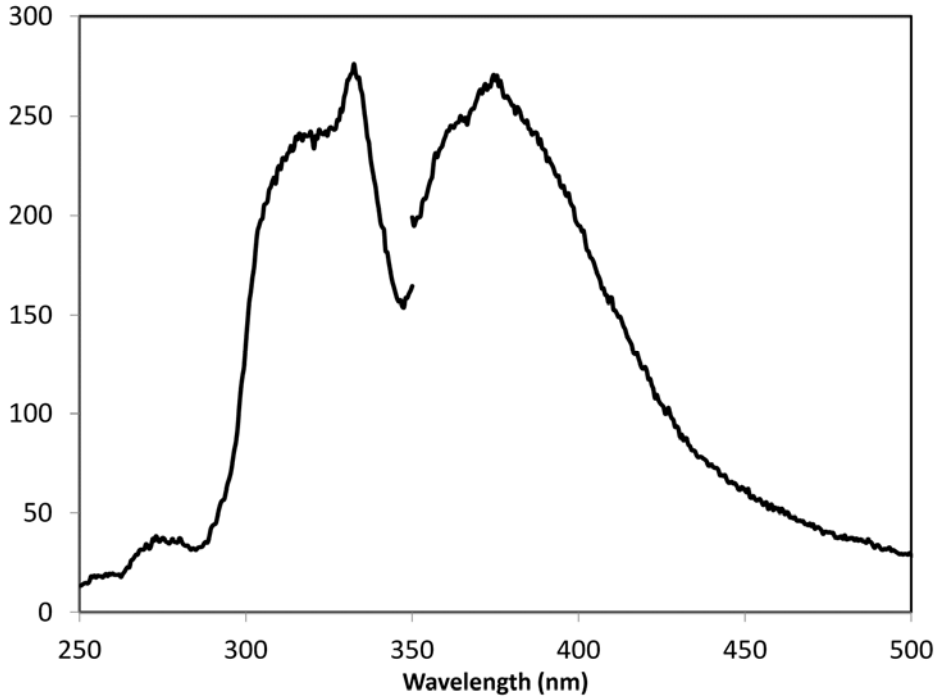

Figure 4.13.1. The emission and excitation spectra of free ligand H_3btc

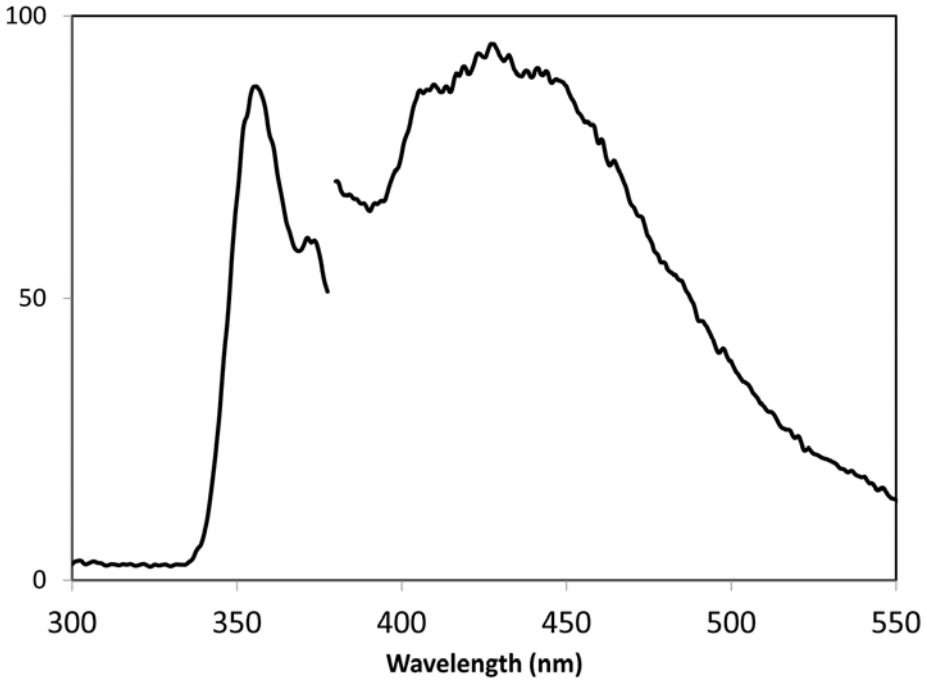

Figure 4.13.2. The emission and excitation spectra of free ligand Hpzc

Infrared spectroscopy

IR (cm^{-1}): 3461s, 3304s, 3204s, 3126s, 1651m (sh), 1611s, 1555s, 1434m, 1378s, 1208w, 1109w, 935(w), 805w, 761m, 720 m, 628w (Figure 4.14).

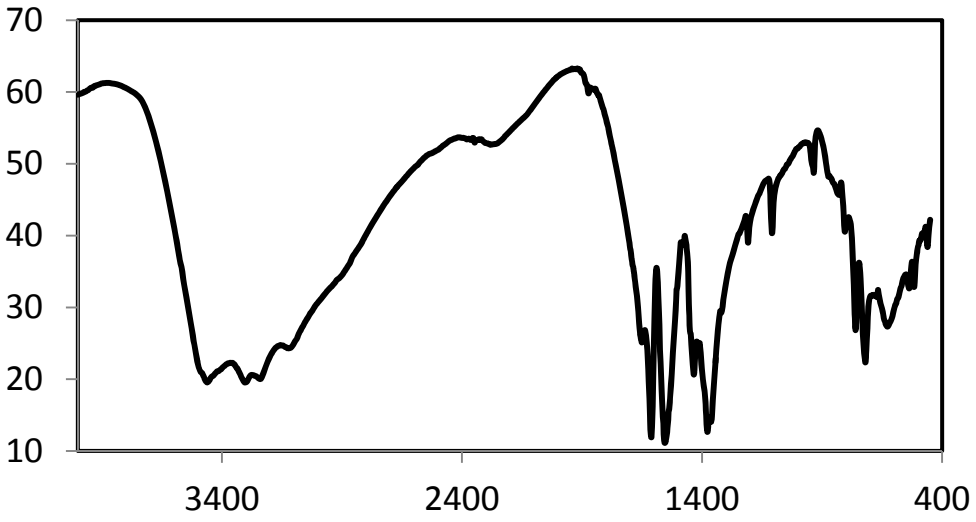

Figure 4.14. IR spectra of compound **1** (KBr).

The O-H stretching over band of 3000-3450 cm^{-1} corresponds to O-H group of water molecule. The two bands around 1651 cm^{-1} and 1611 cm^{-1} can be assigned to C=O stretching because of carboxylic group of H_3btc ligand. The region between 1550 cm^{-1} to 1700 cm^{-1} has stretching due to C=C stretching of benzene ring. The observed bands in range of 700 cm^{-1} to 1200 cm^{-1} can be assigned to C-H and C-C bending of the benzene.

IR (KBr, cm^{-1}): 3342s (br), 1620s, 1551s, 1431s, 1376s, 1162w, 1112w, 1058w, 1037w, 732 m, 663m (Figure 4.15).

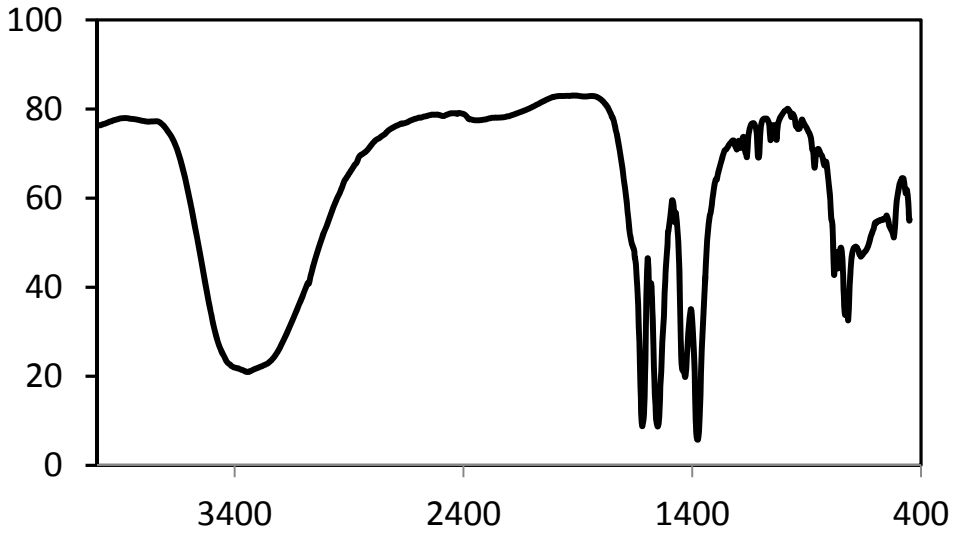

Figure 4.15. IR spectra of compound **2** (KBr).

The O-H stretching over band of 3342 cm^{-1} corresponds to O-H group of water molecule. The bands around 1620 cm^{-1} can be assigned to C=O stretching because of carboxylic group of H_3btc ligand. The bands between 1550 cm^{-1} to 1700 cm^{-1} has stretching due to C=C stretching of benzene ring. The observed bands in range of 700 cm^{-1} to 1200 cm^{-1} can be assigned to C-H and C-C bending of the benzene.

4. Conclusion

Two new metal organic frameworks have been hydrothermally synthesized using s-block metal ions and carboxylate ligands as building units. These compounds are characterized by thermo gravimetric analysis, fluorescent spectra, Uv-visible and infrared spectroscopy. The structure of compound **1** is a three-dimensional framework consisting of helical chains of calcium coordination polymers, while that of compound **2** is a double layered network in which the inorganic zigzag chains of calcium coordination polyhedra are linked by organic ligands. Both compounds show blue fluorescence when excited with UV light.

REFERENCES

1) Long, J. R.; Yaghi, O. M. *Chem. Soc. Rev.*, **2009**, 38, 1213.

2) (a) Rosi, N. L.; Eckert, J.; Eddaoudi, M.; Vodak, D. T.; Kim, J.; O'Keeffe, M.; Yaghi, O. M. *Science* **2003**, *300*, 1127. (b) Dinca, M.; Dailly, A.; Liu, Y.; Brown, C. M.; Neumann, D. A.; Long, J. R. *J. Am. Chem. Soc*. **2006**, *128*, 16876, (c) Collins, D. J.; Zhou, H. C. *J. Mater. Chem*. **2007**, *17*, 3154.

3) (a) Phan, A.; Doonan, C.; Uribe-Romo, F. J.; Knobler, C. B.; O'keeffe, M. and Yaghi, O. M. *Acc. Chem. Res***, 2009**, *43*, 58, (b) D'Alessandro, D. M.; Smit, B. and Long, J. R., *Angew. Chem. Int. Ed*. **2010**, *49,* 6058.

4) Liu, W.; Jiao, T.; Li, Y.; Liu, Q.; Tan, M.; Wang, H.; Wang, L. *J. Am. Chem. Soc*. **2004**, *126*, 2280.

5) Corma, A.; Garcia, H.; and Xamena, F. X. L. *Chem. Rev.*, **2010**, 110 (8), 4606.

6) (a) Yaghi, O. M.; Li, H.; and Groy, T. L. *J. Am. Chem. Soc.* **1996,** *118,* 9096, (b) Platers, M. J.; Howie, R. A. and Roberts, A. J., *Chem. Commun.*, **1997**, 893; (c) Plater, M. J.; Roberts, A. J.; Marr, J.; Lachowski, E. E. and Howie, R. A. *J. Chem. Soc*., *Dalton Trans*., **1998**, 797.

7) (a) Barboiu, M.; Vaughan, G.; Kyritsakas, N.; Lehn, J.-M. *Chem.;Eur. J.* **2003**, *9*, 763. (b) Barboiu, M.; Lehn, J.M. *Proc. Natl. Acad. Sci. U. S. A*. **2002**, *99*, 5201. (c) Dumitru, F.; Petit, E.; van der Lee, A.; Barboiu, M. *Eur. J. Inorg. Chem*. **2005**, *21*, 4255. (d) Barboiu, M.; Petit, E.;Vaughan, G. *Chem.;Eur. J.* **2004**, *10*, 2263.

8) (a) Han, S. S.; Deng, W. Q.; and Goddard, W. A.; *Angew. Chem., Int. Ed*., **2007**, *46*, 6289 (b) Zhang, J.; Wu, T.; Zhou, C.; Chen, S.; Feng, P.; and Bu, X. *Angew. Chem., Int. Ed*., **2009**, *48,* 2542 (c) Sumida, K.; Hill, M. R.; Horike, S.; Dailly, A.; and Long, J. R.; *J. Am. Chem. Soc*., **2009**, 131, 15120 (d) Banerjee, D.; Kim, S. J.; and Parise, J. B., *Cryst. Growth Des.*, **2009**, *9*, 2500 (e) Abrahams, B. F.; Grannas, M. J.; Hudson, T. A.; and Robson, R.; *Angew. Chem., Int. Ed*., **2010**, *49*, 1087 (f) Zhao, X.; Wu, T.; Zheng, S.-T.; Wang, L.; Bu X.; and Feng, P. *Chem. Commun*., **2011**, *47*, 5536.

9) Fromm, K. M., *Coord. Chem. Rev.* **2008**, *252*, 856.

10) Lan, J.; Cao, D.; Wang, W. and Smit, B. *ACS Nano*, **2010**, *4*(7), 4225.

11)Han, S. S. and Goddard, W. A. *J. Am. Chem. Soc.*, **2007**, *129* (27), 8422.
12) (a) Pan, L.; Frydel, T.; Sander, M. B.; Huang, X.; and Li, J., *Inorg. Chem.* **2001**, *40*, 1271, (b) Yang, Y.-Y.; Huang, Z.-Q.; Szeto, L. and Wong, W.-T., *Appl. Organometal. Chem*. **2004**, 18, 97. (c) Nielsen, R. K. B.; Kongshaug, K. O.; Fjellvåg, H., *Solid State Sciences*, **2006**, *8(10)*, 1237. (d) Yang, Y.; Jiang, G.; Li, Y.-Z.; Bai, J.; Pan, Y.; You, X.-Z., *Inorg. Chim. Acta*, **2006**, 359(10), 3257, (e) Fei, Z.; Geldbach, T. J.; Scopelliti, R., and Dyson, P. J., *Inorg. Chem*. **2006**, *45*, 6331, (f) Volkringer, C.; Loiseau, T.; Férey, G.; Warren, J. E.; Wragg, D. S.; Morris, R. E., *Solid State Sciences*, **2007**, 9(6), 455, (g) Shuai, Q.; Chen, S.; Gao, S., *Inorg Chim Acta*, **2007**, 360(5),1381 (h) Williams, C. A.; Blake, A. J.; Wilson, C.; Hubberstey, P., and Schröder, M., *Cryst. Growth Des*., **2008**, 8(3), 911. (i) Volkringer, C.; Marrot, J.; Férey, G., and Loiseau, T., *Cryst. Growth Des*., **2008**, 8(2), 685. (j) Liang, P.-C.; Liu, H.-K.; Yeh, C.-T.; Lin, C.-H. and Zima, V., *Cryst. Growth Des*., **2011**, 11 (3), 699.
13) Ellsworth, J. M. and zur Loye, H.-C., *Dalton Trans.*, **2008**, 5823.
14) SAINT Frame Integration Software; Bruker AXS Inc.: Madison, WI, **2000**.
15) G. M. Sheldrick, & SADABS, Siemens Area Detector Absorption (and other) Correction," Univ. of Göttinger, Göttinger, Germany, **1998**.
16) SHELXTL ver. 6.14, Reference Manual, Bruker Industrial Automation, Analytical Instrument, Madison, WI 53719, **2000**.
17) Sheldrick, G.M., *Acta Cryst.* **2008**, *A64*, 112.
18) International Tables for Crystallography, Vol C, Th. Hahn, Ed. Kluwer Academic Publishers, Holland.
19) Brese, N. E.; O'Keeffe, M. *Acta Crystallogr*. **1991**, *B47*, 192.
20) Ptasiewicz-Bak, H.; Ostrowski, A.; Leciejewicz, J. Pol. J. Chem. **1998** 72, 2014.
21) Chen, W.; Wang, J. Y.; Chen, C.; Yue, Q.; Yuan, H. M.; Chen, J. S.; Wang, S. N. *Inorg. Chem*. **2003**, *42*, 944.
22) Leray, I.; O'Reilly, F.; Habib Jiwan, J.-L.; Soumillion, J.-Ph. and Valeur, B. Chem. Commun., **1999**, 795.

Chapter 5

Two Novel Three-Dimensional Metal-Organic Frameworks Using s-Block Metal Ions as Nodes

1. Introduction

Metal–Organic Frameworks (MOFs) or coordination polymers are crystalline materials composed of metal ions connected by organic linkers forming chain, layer, or 3-D networks.[1, 2] Aromatic polycarboxylate organic linkers are most commonly used due to their structural rigidity and strong binding bonding interactions between metal centers and carboxylate oxygen atoms.[3] MOFs based on the alkali or alkaline earth metals (s-block elements) have been less studied.

In recent years, the focus on alkaline earth metals (Ca, Mg) has been increased and examples based on these metals have been reported.[4] The formation $[Ca(btc)(H_2O)_3]$ network containing zigzag chains of Ca polyhedra under hydrothermal synthesis was previously reported by Matsuzaki[5] and Groeneman.[6] The network was formed by bridging btc linkers and Ca ions. Layered networks have been synthesized under hydrothermal conditions using the btc organic linker. The specific network formed depends on the pH of the solution used in the synthesis.[7,8] For example, $Ca(Hbtc)\cdot 2H_2O$, formed by infinite H-bonded layers of Hbtc dianion, connects in the third dimension though coordinating Ca metal centers. The addition of triethylamine under hydrothermal conditions facilitates complete deprotonation of the linker with the formation of a layered $[Ca_3(btc)_2(H_2O)_{12}]$ network. The aromatic linkers such as bdc, btc, 2-NH_2-btc form 3-D topologies with different CaO motifs under solvothermal conditions.[9]

To date, three calcium/btc based coordination polymers $[Ca_3(btc)_2(H_2O)_{12}]$ (**3**),[10] $[Ca(Hbtc)(H_2O)_2]$ (**4**),[11] $[Ca_3(btc)_2(DMF)_2(H_2O)_2]_3 \cdot 3H_2O$ (**5**),[12] have been reported in the literature. Compounds **3** and **4** are layered structures, while **5** is a 3D framework. Two novel calcium organic frameworks are reported in Chapter 4 in this thesis. Compound **1**, $[Ca_3(btc)_2(H_2O)_{12}]$, represents the second 3D framework constructed from btc and calcium building units. The previously synthesized framework (**3**) has the same formula but it is a layered structure. Compound **2**, $[Ca_2(btc)(pzc)(H_2O)_3]$ (see chapter 4), is a 2D framework formed by the combination of two ligands btc and pzc.

MOFs based on rubidium are relatively less studied. Due to the large electronegativity difference between Rb metal centers and oxygen, Rb-O shows strong ionic character in forming coordination networks. Compounds with general formula $[M_2(bdc)(H_2O)_2]$ [M = Rb, Cs] was reported by Stein[13,14] where Rb and Cs centers are coordinated with four water molecules and four carboxylate oxygen atoms from different terephthalate linkers. Ferey and co-workers[15] recently reported 3D networks of general formula $M_2(TTF\text{-}TC)H_2$ (M = Rb, Cs;TTF-TC= tetrathianfulvalene tetracarboxylate) with redox-active TTF-TC as the organic linkers. Each tetrahedrally coordinated Rb is interconnected through the linkers to form a 3D network. The compound is shown to be thermally stable from 150 -200 °C. Under solvothermal conditions, a dense 3D Rb coordination network using btc linkers have been made by Kim and co-workers.[16] The network contains channels with edge sharing RbO_6 and RbO_8 polyhedral chains surrounding it, connected by the organic linkers. In this chapter, I presented the hydrothermal synthesis of calcium [Ca(Hbtc)(H2O)]•H2O (**6**) and rubidium Rb(Hbdc) (**7**) based 3D frameworks is presented.

2. Experimental Section

Fourier transform infrared spectroscopy

The infrared spectra were recorded from 400 to 4000 cm^{-1} on a Perkin Elmer Spectrum One FTIR spectrometer using KBr pellets.

Thermogravimetric Analysis

The thermogravimetric data were collected on a TA Q5000 TGA instrument at a heating rate of 10°C min^{-1} from room temperature to 800°C in an air atmosphere.

Powder X-ray Diffraction

Powder X-ray analysis was performed on an ARL Thermo X-ray Diffractometer using Cu Kα radiation (1.5418 Å), in which the X-ray tube was operated at 40 kV and 40 mA.

Fluorescence spectra

Fluorescence spectra were obtained by a Perkin Elmer LS55 fluorescence spectrophotometer. The compounds as solid suspensions in water were studied at room temperature. The wavelength used for obtaining the excitation and emission peaks are ranging from 250-350 nm and 350-600 nm respectively.

Synthesis

Compound [Ca(Hbtc)(H_2O)]•H_2O(6)

Compound **6** was synthesized from a mixture of calcium chloride, H_3btc, magnesium nitrate and water. The procedure for the synthesis is: 0.100g $CaCl_2$ and 0.097g $Mg(NO_3)_2$ were dissolved in 1.0 mL of water. To this solution, 1.0 mL of water containing 0.107g of H_3btc was added and stirred for 30 minutes. To the resulting solution 0.5 mL of 2M NaOH is added to make the solution basic. The reaction mixtures

were transferred to Teflon bags, sealed and placed in a 45 mL reaction vessel, and heated in an oven at 150°C for 24 hours. Colorless crystals were filtered and dried overnight in air (yield: 0.117 g, 80%). IR (cm^{-1}): 3544s, 3492s, 3354s, 3257s, 3043s, 2925w, 2664w, 2516w, 1696m, 1612m, 1559s, 1395s, 1269s, 1206m, 1110w, 930w, 855m, 730m, 686w.

Compound Rb(Hbdc) (7)

Compound **7** was synthesized from a mixture of rubidium hydroxide (50% w/w aqueous solution), H_2bdc and water. A typical synthesis is as follows: 0.103 g H_2bdc and 0.387 g of RbOH (50% w/w aqueous solution) were added to 2.0 mL deionized water. After stirring for 30 minutes, 0.5 mL of 2M HCl was added. A white precipitate is formed from the solution. The reaction mixture was transferred to a Teflon cup and placed in a 15 mL reaction vessel, and heated in an oven at 150°C for 48 hours. Colorless needle crystals were filtered and dried in air for overnight (yield: 0.051 g 33 %) IR (cm^{-1}): 3443s, 3052w, 2508w, 1973w, 1719s, 1504m, 1391w, 1297m, 1233m, 1117w, 895s, 745s, 509m.

X-ray Crystallography

X-ray diffraction data for compounds **6** and **7** were collected on a Bruker Quazar diffractometer with an Apex II CCD area detector. The data was processed with the SAINT software[17] and corrected for absorption with SAD-ABS.[18] The structure was solved by direct methods SHELXTL V.6.10 package[19] and was refined against F^2 by weighted full-matrix least-squares calculations.[20] All non-hydrogen atoms were refined allowing for anisotropic displacement. Hydrogen atoms were localized from the difference fourier maps. Atomic scattering factors were taken from the International

Tables for Crystallography.[21] Crystal data and relevant details of the structure determinations are summarized in Table 5.

3. Results and Discussion

Synthesis

Calcium chloride when reacted benzene tricarboxylic acid forms [Ca(Hbtc)•H_2O]. Adding NaOH to the reaction mixture help the deprotonation of H_3btc and the formation of the $Hbtc^{2-}$ anion. In this reaction, $Mg(NO_3)_2$ was added but did not present in the compound **6**. However, $Mg(NO_3)_2$ in the reaction mixture is necessary for the crystallization of compound **6**.

The formation of compound **7** is an acid-base reaction between rubidium hydroxide and benzene-1, 4-dicarboxylic acid. The resulting salt [Rb(Hbdc)] is not soluble in water. Thus the pH of the reaction mixture is very important for the crystallization of this compound. An acidic medium would help to slow the crystallization of the salt to form crystals.

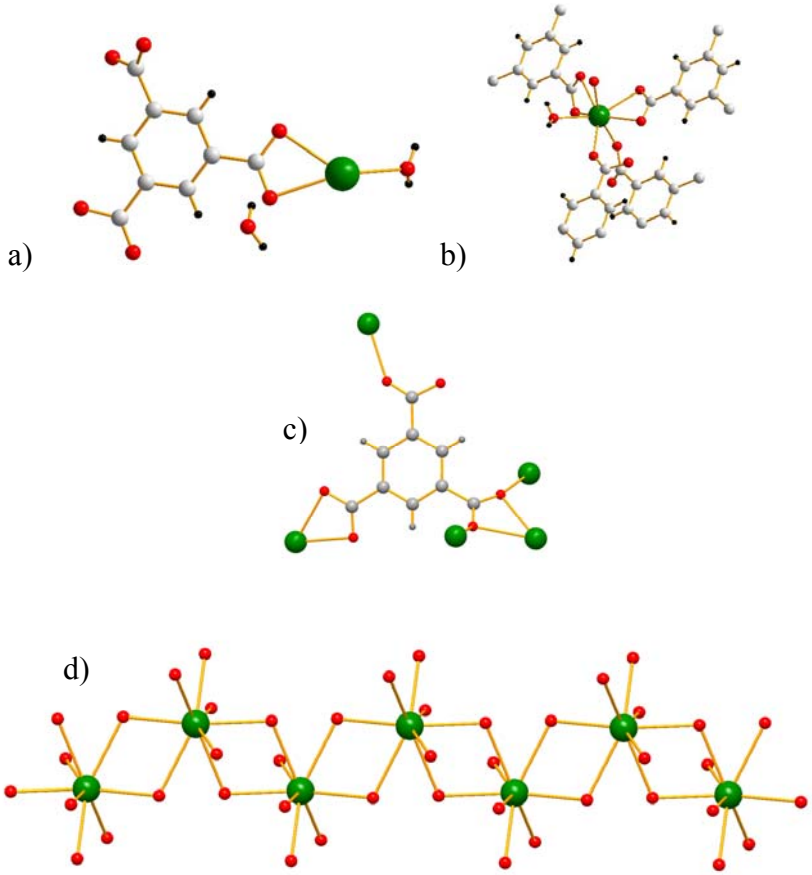

Figure 5.1. a) asymetric unit; b) the coordination Ca; c) coordination of btc environment; d) 1D inorganic chain of {CaO8}

Structure description of compound 6

The structure of compound **6** is a three-dimensional framework consisting of Ca ions, btc ligands and coordinated waters. Its asymmetric unit consists of one Ca ion, one btc ligand and two water molecules. The coordination number for calcium is eight. Each Ca ion binds to one water molecule and seven carboxylate oxygens of seven btc ligands to form $\{CaO_8\}$ polyhedra. The Ca-O bond lengths are in the range of 2.405 – 2.572Å. The btc ligand coordinates to five Ca atoms with its three carboxylate groups. Two of the

three –COO groups are almost coplanar with the benzene ring of btc, while the third is out of plane (dihedral angle 43.73(3)°).

Adjacent $\{CaO_8\}$ polyhedra are edge-shared to give a one dimensional inorganic chain along the *a* direction. In the chain, neighboring Ca…Ca distances are 4.1060(2) and 4.0380 (2)Å alternatively.

Table 5.1. Crystal data and structure refinements for 1-2

	6	7
Formula	C_9 H_7 Ca O_8	C8 H5 O4 Rb
Mol. wt.	283.23	249.58
Crystal system	Triclinic	Monoclinic
Space group	P -1 (2)	C 1 2/c 1 (15)
a (Å)	6.8431(1)	18.7986(3)
b(Å)	8.9881(2)	3.8462 (1)
c(Å)	9.9755(2)	11.4314(2)
α(°)	102.096 (1)	90
β(°)	100.554(1)	96.761 (1)
γ(°)	110.170(1)	90
V($Å^3$)	540.90 (2)	820.78(3)
Z	2	8
Wavelength(Å)	0.71073	0.71073
Temperature(K)	296	296

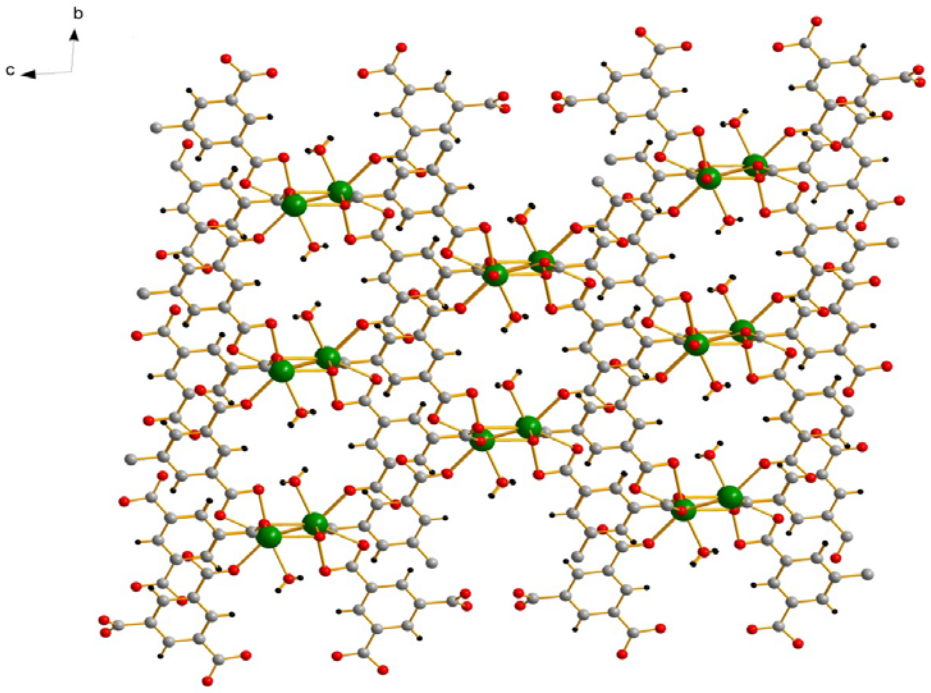

Figure 5.2. 3D crystal structure of compound **6**

Figure 5.2 shows the crystal structure of compound **6** viewed along the *a* direction. Each inorganic chain of $\{CaO_8\}$ polyhedra is connected by btc ligands to six other inorganic chains of $\{CaO_8\}$ polyhedral to form a 3D framework structure with one-dimensional channels along the *a* direction. Each calcium atom bonds to one water molecule (O(2w)) which points into the channels. The uncoordinated water molecule (O(1w)) is located in the channel and form hydrogen bonds with O(2w). These water molecules can be potentially removed to produce porous framework.

Structure description of Compound 7:

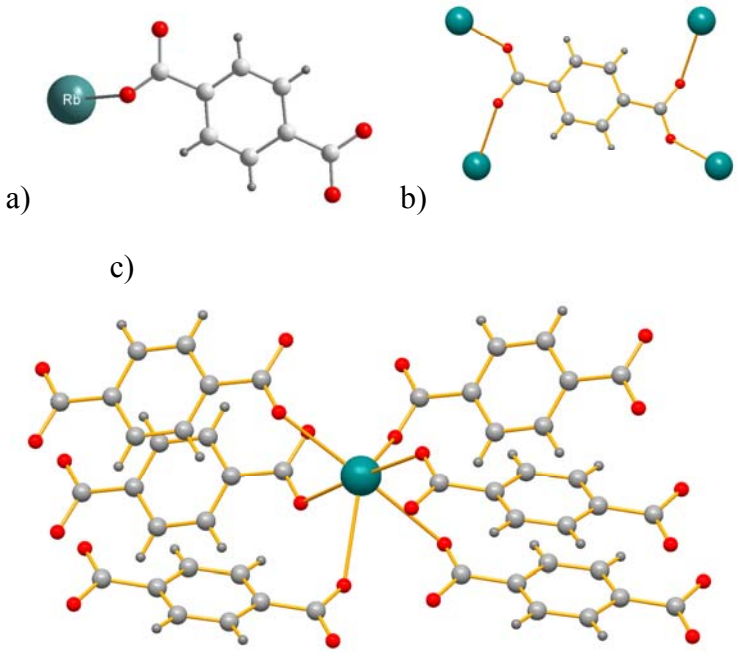

Figure 5.3. (a) asymmetric unit ; (b) bdc coordination environment; (c) rubidium coordination environment

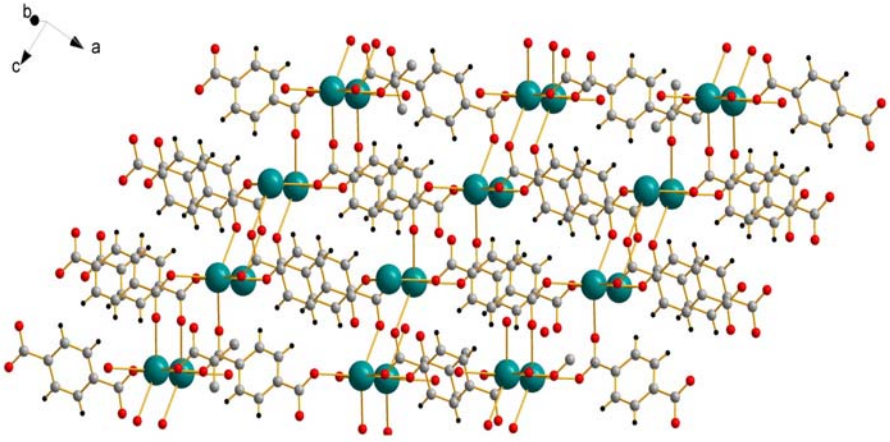

Figure 5.4. The 3 dimensional crystal structure of the compound **7**.

The structure of compound **7** is a 3D dimensional structure consisting of Rb ions and bdc ligands. The asymmetric unit consists of one half Rb ion and one half btc. Each rubidium atom bonds to six carboxylate oxygens of six bdc ligands. The Rb-O bond lengths are in the range of 2.823 Å -2.98 Å. Figure 5.3 shows the crystal structure of compound 7, which is viewed along the b direction. The structure can be viewed as Rb ions connected by carboxylate groups to form layers parallel to the bc plane. The layers are in turn connected by the benzene rings to form a 3D framework structure. One dimensional inorganic chains are formed along the *b* direction with Rb ions connected by carboxylate oxygens.

3.1 Thermo gravimetric Analysis

To study the thermal stability, thermogravimetric analysis was performed on both compounds (Figure 5.5). A crystalline sample was heated from 30 to 900 °C in air at a heating rate of 10 °C /min.

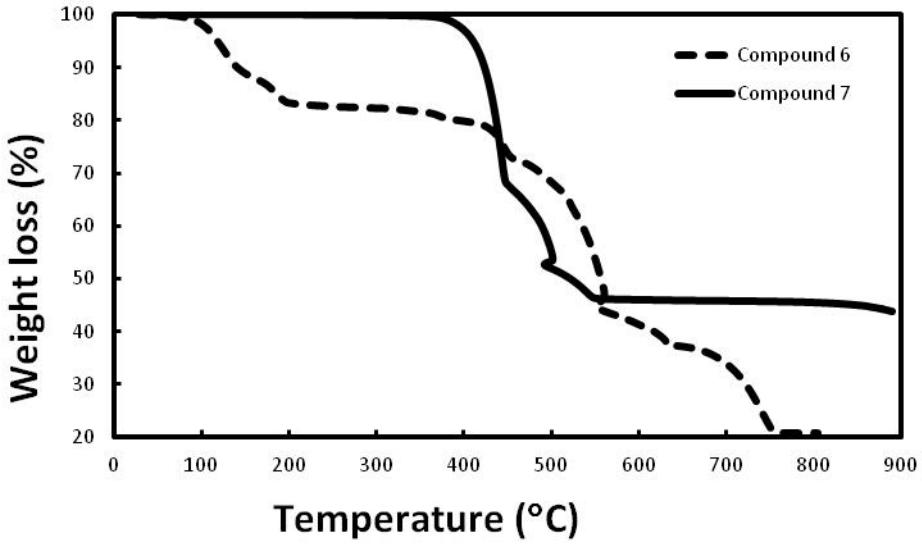

Figure 5.5. The Thermogravimetric analyses of compounds **6** and **7**.

A crystalline sample was heated from 30 to 900°C in air at a heating rate of 10°C /min. An initial weight loss of approximately 16.9% at 40-200°C was observed for compound **6**. In between 450-800°C, a weight loss of 69.1% is observed in three steps. This is attributed to the decomposition of the btc ligand.

As for compound **7**, there was no weight loss up to 400°C. From 400 – 600°C, a weight loss of 54.2% is observed in two steps. This is caused by the decomposing and removal of bdc ligands.

3.2. Fluorescence

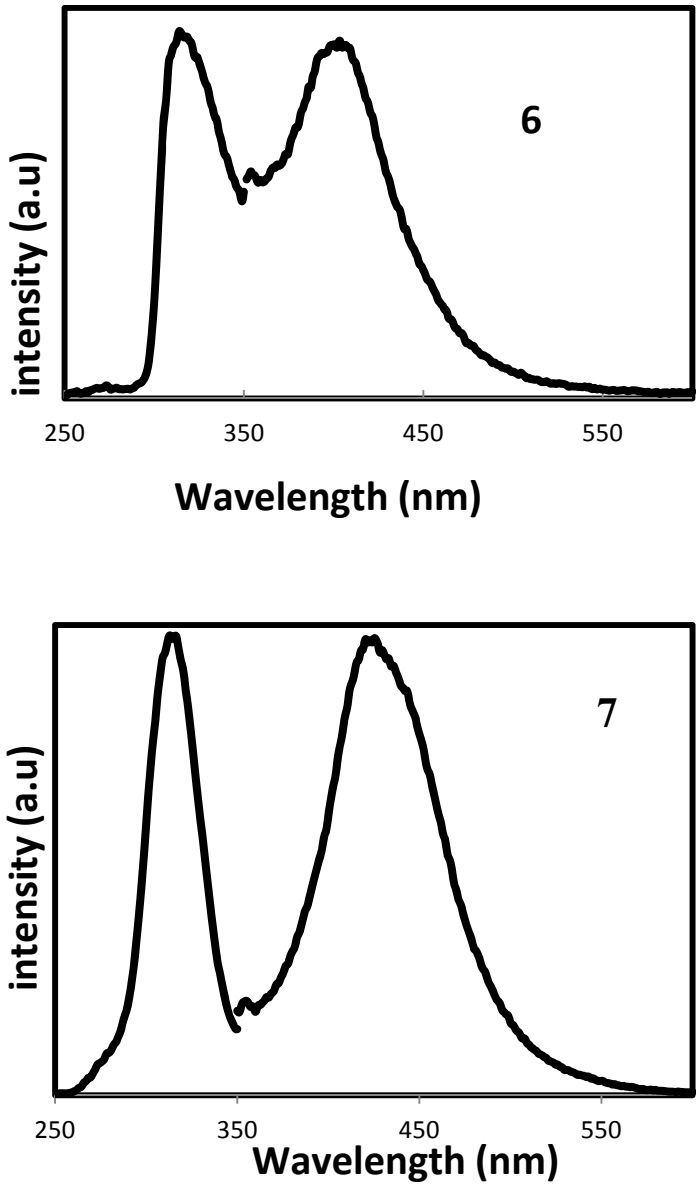

Figure 5.6. The excitation-emission spectra of compound **6** and compound **7** at room temperature.

When excited at 334 nm, the free H_3btc ligand shows the emission λmax of 370 nm, which can be assigned to π*-n transitions. When the btc ligand coordinated to Ca^{2+} ions in the coordination polymers, the emission λmax for **6** have shifted to 404 nm. A blue shift for the excitation λmax for 6 was observed.

The free H_2bdc ligand shows the strongest emission peak at 380 nm with the excitation peak at 340 nm at room temperature, which can be assigned to π*-n transitions. Compared to the free ligands, the strongest excitation peak for compound **7** is at 317 nm, with energy higher than that of the H2bdc ligand. The emission spectrum of compound 7 shows one strong peak at 427 nm.

3.3. Infrared Spectroscopy

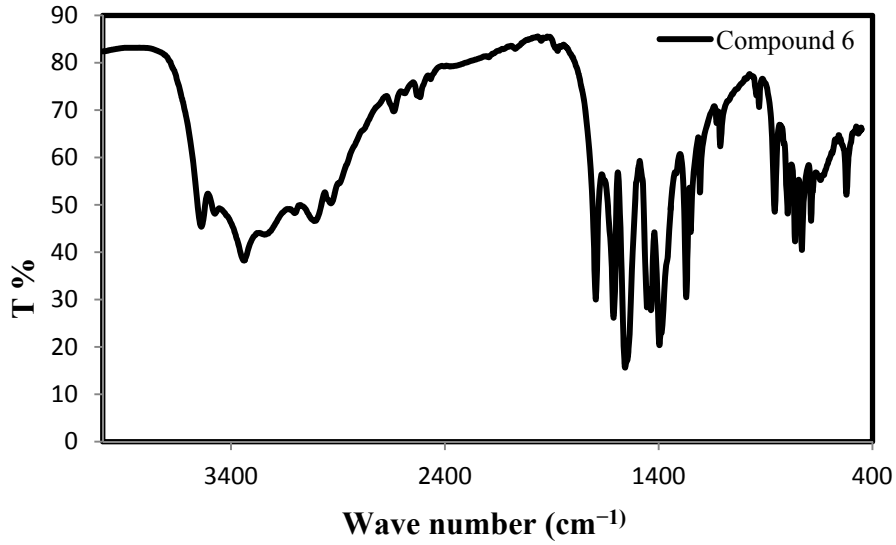

Figure 5.7. IR spectra of compound **6** (KBr)

The O-H stretching over band of 3000-3450 cm^{-1} corresponds to O-H group of water molecule. The two bands around 1696 cm^{-1} and 1612 cm^{-1} can be assigned to C=O stretching because of carboxylic group of H_3btc ligand. The region between1400 cm^{-1} to 1600 cm^{-1} has stretching due to C=C stretching of benzene ring. The observed bands in range of 800 cm^{-1} to 1400 cm^{-1} can be assigned to C-H bending of the benzene.

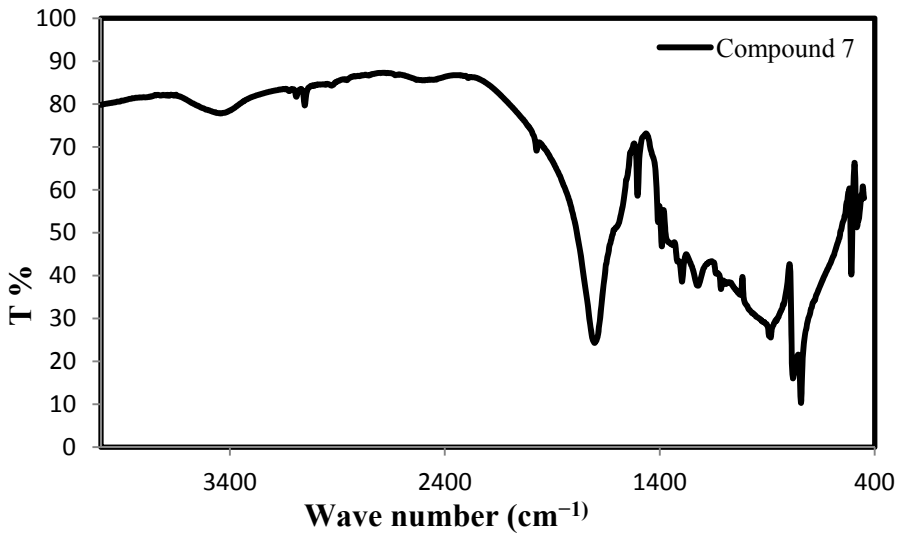

Figure 5.8. IR spectra of compound **7** (KBr)

The O-H stretching is not observed in the band range 3000-3400 cm^{-1} because of absence of water molecules in this compound. The band observed at 1719 cm^{-1}can be assigned to C=O stretching because of carboxylic group of BDC ligand. The vibrational bands in the range of 800 – 1300 cm^{-1} can be assigned to out of plane vibrations of terephthalates.

4. Conclusion

Two novel 3D MOFs (compounds **6** & **7**) based on s-block based metal ions have been synthesized and characterized by Single crystal X-ray diffraction, thermo gravimetric analysis, fluorescent spectra and Infrared spectroscopy. Compound **6** is a porous framework and contains water molecules in the pores. Compound **7** has 3D structure but it does not have any pores.

REFERENCES

1) Cheetham, A. K.; Rao, C. N. R.; Feller, R. K. *Chem. Commun*. **2006**, 4780.

2) Fromm, K. M. *Coord. Chem. Rev*. **2008**, 252, 856.

3) Park, H.; Britten, J. F.; Mueller, U.; Lee, J.; Li, J.; Parise, J. B.*Chem. Mater*. **2007**, 19, 1302.

4) Fromm, K. M., *Coord. Chem. Rev.* **2008**, *252*, 856.

5) Matsuzak, T.; Iitaka, Y. *Acta Crystallogr*. B 1972, B28, **1977**.

6) Groeneman, R. H.; Atwood, J. L. *Cryst. Eng*. **1999**, 2, 241.

7) Platers, M. J.; Howie, R. A.; Roberts, *A. J. Chem. Commun*. **1997**, 893.

8) Yang, Y. Y.; Huang, Z. Q.; Szeto, L.; Wong, W. T. *Appl. Organomet. Chem*. **2004**, 18, 97.

9) Liang, P. C.; Liu, H. K.; Yeh, C. T.; Lin, C. H.; Zima, V. *Cryst. Growth Des*. **2011**, 11, 699.

10) Yang, Y.-Y.; Huang, Z.-Q.; Szeto, L. and Wong, W.-T., *Appl. Organometal. Chem*. 2004, 18, 97.

11) Platers, M. J.; Howie, R. A.; Roberts, A. J. *Chem. Commun*. **1997**, 893.

12) Liang, P.-C.; Liu, H.-K.; Yeh, C.-T.; Lin, C.-H.; Zima, V., *Cryst. Growth Des*., **2011**, 11 (3), 699.

13) Stein, I.; Ruschewitz, U. *Acta Crystallogr*., E **2006**, 62, M2116.

14) Stein, I.; Ruschewitz, U. *Acta Crystallogr*., E **2007**, 63, M382.

15) Nguyen, T. L. A.; Demir-Cakan, R.; Devic, T.; Morcrette, M.; Ahnfeldt, T.; Auban-Senzier, P.; Stock, N.; Goncalves, A. M.; Filinchuk, Y.; Tarascon, J. M.; Ferey, G. *Inorg. Chem.* **2010**, 49, 7135.

16) Kim, M. K.; Jo, V.; Lee, D. W.; Shim, I. W.; Ok, K. M. CrystEngComm **2010**, 12, 1481.

17) SAINT Frame Integration Software; Bruker AXS Inc.: Madison, WI, **2000**.

18) Sheldrick, G.M.; SADABS, Siemens Area Detector Absorption (and other) Correction," Univ. of Gottinger, Gottinger, Germany, **1998**.

19) SHELXTL ver. 6.14, Reference Manual, Bruker Industrial Automation, Analytical Instrument, Madison, WI 53719, **2000**.

20) Sheldrick, G.M. *Acta Cryst.* **2008**, *A64*, 112.

21) International Tables for Crystallography, Vol C, Th. Hahn, Ed. Kluwer Academic Publishers, Holland.

Chapter 6

Conclusion

Four new MOFs based on s-block metal ions have been synthesized using the hydro/solvothermal method: three new calcium based MOFs [$(Ca_3(btc)_2(H2O)_{12}$] $Ca_2(btc)(pzc)(H_2O)_3$, [$Ca(Hbtc)(H_2O)$]•H_2O and one new Rb based MOF [Rb(Hbdc)]. The structure of compound [$(Ca_3(btc)_2(H2O)_{12}$] is a three-dimensional framework consisting of helical chains of calcium coordination polymers. [$Ca_2(btc)(pzc)(H_2O)_3$] is a double layered network in which the inorganic zigzag chains of calcium coordination polyhedra are linked by organic ligands. [$Ca(Hbtc)(H_2O)$]•H_2O is a 3D framework structure with one-dimensional channels along the *a* direction. The [Rb(Hbdc)] compound has a 3D structure and it is not a porous material. These compounds are characterized by Single Crystal X-ray Diffraction, Powder X-ray Diffraction, thermo gravimetric analysis, fluorescent spectra and Infrared spectroscopy.